Solution of the time-dependent Schrödinger equation using uniform complex scaling

Jakob Bengtsson, Eva Lindroth, and Sølve Selstø

Atomic Physics, Fysikum, Stockholm University, AlbaNova University Center, SE-106 91 Stockholm, Sweden
(Received 20 March 2008; published 3 September 2008)

The formalism of complex rotation of the radial coordinate is studied in the context of time-dependent systems. The applicability of this method is discussed and illustrated with numerical examples involving atoms exposed to electromagnetic field pulses. Complex rotation proves to be an efficient tool to obtain ionization probabilities and rates. Although, in principle, any information about the system may be obtained from the rotated wave function by transforming it back to its unrotated form, a good description of the ionized part of the wave function is generally subject to numerical challenges. It is, however, found that the combination of complex rotation and Floquet formalism offers an alternative and promising possibility to retrieve the physical information.

I. INTRODUCTION

To describe processes induced when atomic systems interact with electromagnetic fields or with impinging particles, an adequate description of excited states is necessary. Of special interest are resonance states. These are states that are mainly localized, but with a coupling to the continuum. The coupling can be due to the electron-electron interaction (the Auger effect), as well as to static or time-dependent external fields (field ionization). The large spatial overlap between resonance states and bound states can result in substantial transfer of population from the latter to the former when the system absorbs energy. Due to the coupling to the continuum, the net result is an efficient path to ionization, often manifested in strong resonances in ionization spectra.

A widespread theoretical approach to handle resonance states is that of complex scaling (also called complex rotation), see, e.g., Refs. [1,2]. The radial coordinate is then scaled by a complex phase factor, and as a consequence the energy positions and half widths of the resonances are obtained as real, respectively, imaginary parts of complex eigenvalues to a non-Hermitian Hamiltonian matrix. The imaginary part, the half width, gives directly the transition rate from the localized part of a resonance state due to the coupling to the continuum. For states that decay through Auger emission the method has, in its traditional form of *uniform scaling*, been combined with a number of calculation schemes such as Hylleraas wave functions [3–5], configuration interaction [6], many-body perturbation theory [7–9], parametric coordinates [10,11], or the hyperspherical harmonic method [12]. Most studies have focused on the determination of resonance parameters, but the method has also been employed to calculate resonances in the photoabsorption cross section [13–15] as well as electron-ion recombination cross sections, both in a nonrelativistic and a relativistic framework [16–25]. Also states that couple to the continuum due to the interaction with a static electric field have been successfully treated with complex rotation [26–28]. Here, as in the case of Auger decay, it is a time-independent interaction that causes the decay. The interaction between an atom and an ac field is in contrast time-dependent. With the Floquet formalism by Shirley [29] it was shown that the com-

bined atom-field system can, for a time-periodic field, anyhow be characterized by eigenstates and eigenvalues of a *time-independent*, albeit in principle infinite-dimensional, matrix. Upon diagonalization of this matrix the atom-field interaction is included nonperturbatively; the atomic states are *dressed* by the field. The combination of the Floquet approach with complex rotation, proposed by Chu, Reinhardt, and co-workers [26,30,31], allowed for an efficient inclusion of the field-induced coupling to the continuum. As in the time-independent case, this results in complex eigenvalues (this time to the Floquet Hamiltonian matrix) and again the imaginary parts give the transition rate to the continuum. This combination has since then successfully been used to examine various strong field phenomena, a rather recent review can be found in Ref. [32].

An alternative to the *uniform* complex scaling (used in the studies mentioned so far) is *exterior complex scaling*, where the scaling of the coordinates starts at some finite distance from the origin. Also this method has been applied to obtain resonance parameters in connection with electronic autoionization [33,34], but it has been even more utilized to obtain cross sections for electron impact ionization [35,36], and nonresonant photoionization [37,38]. The key interest here has not been the calculation of resonances, but to profit from the fact that the complex scaling at large radial distances can act as an absorbing boundary while at the same time the unscaled inner region allows extraction of cross sections in the same manner as with real coordinates.

The last decade has seen a rapid development of the ability to produce laser pulses of shorter and shorter time duration. Furthermore, the free-electron facilities coming into operation will provide pulses that are also highly energetic. Due to this development, experimental studies of several atomic processes can nowadays be made in the time domain. Naturally, this development has been accompanied by theoretical efforts to handle truly time-dependent Hamiltonians and to model the time-evolution of the wave functions. For this several successful schemes aiming for straightforward solutions to the time-dependent Schrödinger equation have been developed, involving both basis sets and finite difference methods, see, e.g., Refs. [39–41].

The first authors that used the method of complex scaling together with explicit time propagation of wave packets were

McCurdy *et al.* [42,43], who argued [43] that the *key to practical applications of complex coordinates to time dependent problems* is exterior complex scaling. More recent studies using the same approach can be found in Refs. [44,45]. However, 10 years ago Scrinzi and Piraux [46], in a calculation on two-electron atoms exposed to short intense laser pulses, demonstrated convincingly that also uniform complex scaling may fruitfully be applied to study dynamics. Later related studies can be found in Refs. [47,48]. Regarding the combination of the Floquet approach and complex scaling, few attempts seem to have been made to use it to study explicit time evolution, although an important exception is the work by Buchleitner *et al.* [49].

The most obvious benefit from complex rotation is the ability to account for effects due to resonances when an atom is exposed to time-dependent perturbations. However, as we will demonstrate, the method has additional advantages which are valuable also in the absence of resonances. For instance, convergence with respect to the number of basis states is achieved with surprisingly few states for uniform complex scaling. The purpose of the present work is to further investigate the possibilities with this type of scaling. We have used three different procedures, all based on uniform complex rotation, to solve the time-dependent Schrödinger equation for our model system; the hydrogen atom exposed to a short laser pulse. Two of the methods solve the time-dependent Schrödinger equation directly, while the third method utilizes the Floquet formalism. The basic concepts with complex rotation are reviewed and discussed in relation to the solution of explicitly time-dependent problems in Sec. II. We penetrate especially the question of what information can be obtained from the time-propagated complex rotated wave function. In this respect we show, in Sec. III C, that the Floquet formalism offers unique possibilities. Numerical examples supporting these findings are shown in Sec. IV, where also solutions with and without complex rotation are compared, and the dramatically improved convergence for the latter is discussed.

II. COMPLEX ROTATION

In this section we review and discuss the proper calculation of different quantities with complex rotation. Of special interest is the form of the inner product. This has earlier been discussed in detail by Moiseyev *et al.* [50], who introduced the label *c product*. A later study focused on the time-dependent case [51]. As will be discussed below our conclusions about the inner product in a time-dependent framework differ from those of Ref. [51].

The complex rotation of the Hamiltonian, $H \rightarrow H^\theta$, is usually performed by a direct transformation of the radial variable

$$r \rightarrow r e^{i\theta}. \qquad (1)$$

A well-studied example is the one-particle hydrogenlike Schrödinger equation without external fields which transforms as

$$H = \frac{\mathbf{p}^2}{2m} - \frac{Ze^2}{4\pi\varepsilon_0 r} \rightarrow H^\theta = \frac{\mathbf{p}^2}{2m} e^{-2i\theta} - \frac{Ze^2}{4\pi\varepsilon_0 r} e^{-i\theta}. \qquad (2)$$

For the discussion on complex rotation it is useful to note that the same transformation can be obtained through the rotation operator $\exp(\hat{A})$ [49], where

$$\hat{A} \equiv \frac{-\theta(\mathbf{r} \cdot \mathbf{p} + \mathbf{p} \cdot \mathbf{r})}{2\hbar}. \qquad (3)$$

To see this we apply $\exp(\hat{A})$ from the left to the time-independent Schrödinger equation

$$e^{\hat{A}} H \Psi(\mathbf{r}) = E e^{\hat{A}} \Psi(\mathbf{r}). \qquad (4)$$

Noting that $\exp(-\hat{A})$ is the inverse of $\exp(\hat{A})$, we insert unity in the form of $\exp(-\hat{A})\exp(\hat{A})$,

$$e^{\hat{A}} H e^{-\hat{A}} e^{\hat{A}} \Psi(\mathbf{r}) = E e^{\hat{A}} \Psi(\mathbf{r}). \qquad (5)$$

With the help of the Baker-Hausdorf lemma [52],

$$e^{\hat{A}} H e^{-\hat{A}} \equiv H + [A,H] + \frac{1}{2!}[A[A,H]] + \frac{1}{3!}[A,[A,[A,H]]] + \cdots, \qquad (6)$$

it is readily shown that

$$e^{\hat{A}} H e^{-\hat{A}} \equiv H^\theta \qquad (7)$$

for any Hamiltonian, H, that can be written as sums of the operators $\mathbf{r}^n$ and $\mathbf{p}^n$, with n being a positive or negative integer. In particular, this is true for the atomic Schrödinger Hamiltonian in the presence of an electromagnetic field expressed in either length or velocity gauge, see further Sec. III. We thus have

$$H^\theta e^{\hat{A}} \Psi(\mathbf{r}) = E e^{\hat{A}} \Psi(\mathbf{r}) \qquad (8)$$

and it is obvious that $\exp(\hat{A})\Psi(\mathbf{r})$ is an eigenfunction to H^θ with eigenvalue E. The rotated eigenfunction, $\Psi(\mathbf{r}e^{i\theta})$, must then, up to a possible constant, be obtained from the application of $\exp(\hat{A})$ on $\Psi(\mathbf{r})$. From the fact that the operator $\hat{A}$ can be rewritten as

$$\hat{A} = -\frac{\theta}{\hbar}\mathbf{r} \cdot \mathbf{p} - \frac{\theta}{2\hbar}[\mathbf{p},\mathbf{r}] = i\theta\mathbf{r} \cdot \nabla + \frac{i3\theta}{2} \qquad (9)$$

and since $\exp(i\theta\mathbf{r}\cdot\nabla)\mathbf{r} = \mathbf{r}\exp(i\theta)$, which can be seen from a Taylor expansion of the exponential operator, it is possible to find this constant;

$$e^{\hat{A}}\Psi(\mathbf{r}) = e^{i3\theta/2}\Psi(\mathbf{r}e^{i\theta}). \qquad (10)$$

This constant assures that a normalized function stays normalized after rotation as will be seen below. Similarly, a rotated wave function can be transformed back to the unrotated one through the inverse transformation

$$e^{-\hat{A}}\Psi(\mathbf{r}e^{i\theta}) = e^{-i3\theta/2}\Psi(\mathbf{r}). \qquad (11)$$

Note finally that the eigenenergy, E, in Eq. (8) is *not* affected by the rotation.

The rotation operator can now be used to investigate the connection between calculations with and without complex rotation. We start with how the inner product should be calculated with rotated wave functions, a question that has been discussed in quite some detail in the literature, see, e.g., Ref. [51]. Starting with the expression used for ordinary unrotated wave functions in the Hermitian formulation of quantum mechanics,

$$\int \Phi^*(\mathbf{r})\Psi(\mathbf{r})dV, \tag{12}$$

we insert unity in the form of the rotation operators

$$\int \Phi^*(\mathbf{r})e^{-\hat{A}}e^{\hat{A}}\Psi(\mathbf{r})dV = \int [(e^{-\hat{A}})^{\dagger}\Phi(\mathbf{r})]^*e^{\hat{A}}\Psi(\mathbf{r})dV. \tag{13}$$

For wave functions Φ and Ψ that vanish asymptotically, this equals

$$\int [e^{-\hat{A}}\Phi(\mathbf{r})]^*e^{\hat{A}}\Psi(\mathbf{r})dV, \tag{14}$$

since $\hat{A}$ is Hermitian. From Eq. (3) it is clear that if $\exp(\hat{A})$ rotates the wave function with θ, $\exp(-\hat{A})$ rotates it with $-\theta$. The expression in Eq. (14) can thus be written in coordinate form as

$$\int \Phi^*(\mathbf{r}e^{-i\theta})\Psi(\mathbf{r}e^{i\theta})dVe^{3i\theta}, \tag{15}$$

where the complex constant follows from Eqs. (10) and (11). We note that with this constant it is also clear that for normalizable states, complex rotation will be equivalent to a variable transformation through Cauchy's theorem. In addition, although the choice of normalization is to some extent arbitrary, it is convenient that a wave function normalized according to the usual inner product in Eq. (12) stays normalized after complex rotation. It is finally worth noting that if the unrotated wave function, $\Phi(\mathbf{r})$, is real, then $\Phi^*(\mathbf{r}e^{-i\theta})$ will be equal to $\Phi(\mathbf{r}e^{i\theta})$, i.e., the inner product will be calculated as

$$\int \Phi(\mathbf{r}e^{i\theta})\Psi(\mathbf{r}e^{i\theta})dVe^{3i\theta}. \tag{16}$$

This is the type of inner product always used in complex rotation calculations, although often stated in a less formal way. As an example Ref. [13] expresses it as "Φ^* is defined by taking the complex conjugate of all angular functions, but not of the radial coordinates." This inner product is, except for the explicit appearance of the factor $\exp(3i\theta)$, what Moiseyev and co-workers have labeled the *c product*, see Refs. [50,51,53–55].

One might think that the question how to calculate inner products after complex rotation is solved with the expression in Eq. (15). The situation is, however, somewhat more complicated. This complication is related to how calculations are performed in practice. In a practical calculation the goal is generally to obtain a *finite* number of solutions to a given

Hamiltonian. The calculation is consequently usually confined to a space that is finite, but still adequate to describe the desired solutions. Typically this means that it is restricted in r, for example, restricted to a box with $r < R$, and that it allows only a finite number of nodes. As a consequence of these restrictions, the space can now be spanned by a finite basis set. The expansion in such a basis set can be found by diagonalization of a matrix representation of the Hamiltonian in the finite space. It is important to notice that the space restrictions imply a modification of the Hamiltonian. If, for example, the calculation is constrained to a space $r < R$, this is equivalent to the addition of a potential $V(r) \rightarrow \infty$ for $r \geqslant R$. The original Hamiltonian and that of which we have a matrix representation will in fact only have some eigenstates in common, namely those of the original Hamiltonian for which the space is adequate. The Hamiltonian obtained when the space is restricted is further not possible to rotate as in Eq. (7) since the implicitly added potential destroys the equivalence between this rotation and the Hamiltonian rotated through $r \rightarrow r \exp(i\theta)$ as in Eq. (2). One clear manifestation of this is that although the eigenvalues to the true rotated Hamiltonian, Eq. (8), are real, those of its finite space matrix representation, $\mathbb{H}^{\theta}$, are generally complex. The fact that this complexity arises due to the use of a restricted space can be seen as follows. The asymptotic form of the continuum solutions to the Schrödinger equation for hydrogenlike systems is proportional to

$$\sim \sin\left(kr - \frac{Z}{ka_0}\ln(2kr) - \frac{\ell\pi}{2} + \sigma_\ell\right), \tag{17}$$

where a_0 is the Bohr radius and σ_ℓ is the Coulomb phase shift. The requirement that all eigenvectors should vanish at the border of a finite space, R, i.e.,

$$\Psi(r = R) = 0, \tag{18}$$

leads to a quantization of k. When $r \rightarrow r \exp(i\theta)$, Eq. (17) transforms to

$$\sim \sin\left(kre^{i\theta} - \frac{Z}{ka_0}\ln(2kre^{i\theta}) - \frac{\ell\pi}{2} + \sigma_\ell\right). \tag{19}$$

For Eq. (18) still to hold, k must be rotated into the complex plane so that it compensates the rotation of r. For $Z = 0$ this amounts to a transformation $k \rightarrow k \exp(-i\theta)$, leading to

$$E_k \rightarrow E_k e^{-2i\theta}. \tag{20}$$

For $Z \neq 0$ the relation in Eq. (20) is an approximation. It improves with increasing k, however. Hence it is the combination of complex rotation and *boundary conditions* that results in complex energies for the pseudocontinuum. Although well-known, see, e.g., Ref. [56], this is not always pointed out in the literature on complex rotation.

We conclude thus that Eq. (7) does not hold for a Hamiltonian that we can represent with a matrix, and consequently a general eigenstate to the rotated matrix representation cannot be obtained through operation with $\exp(\hat{A})$. Again, only those eigenstates for which the space is adequate, obey the relation in Eq. (8). This might seem as a severe limitation, but in practice all interesting cases fall into this category.

First, any bound state can be well-described in a finite space (although this finite space may still have to be large). Second, an outgoing wave packet, representing, e.g., an electron leaving the system, can for a finite time be well-represented in a finite space.

A. Calculating the eigenfunctions in a finite space

When we want to work with a matrix representation of the Hamiltonian, it is reassuring to know that the form of the inner product follows directly from matrix algebra and is a consequence of the symmetry of the matrix. A general diagonalizable $n \times n$-matrix has n right (column) eigenvectors, $\mathbf{R}_i$, corresponding to n eigenvalues, λ_i. It has also n left (row) eigenvectors, $\mathbf{L}_i$, corresponding to the same n eigenvalues. Left and right eigenvectors associated with different eigenvalues are orthogonal to each other, i.e., $\mathbf{L}_i \cdot \mathbf{R}_j = 0$ if $\lambda_i \neq \lambda_j$. As is well-known, the left eigenvector of a symmetric matrix (real or complex) is identical to the transpose of the corresponding right eigenvector, while for a Hermitian matrix it also has to be complex conjugated. Below we derive a general relation between right and left eigenvectors to any matrix representing an initially Hermitian operator that has been complex rotated. The matrix representation of an unrotated Hermitian operator is a Hermitian matrix $\mathbf{B}$;

$$\mathbf{B} = \mathbf{B}_{\mathrm{Re}} + i\mathbf{B}_{\mathrm{Im}}, \tag{21}$$

where $\mathbf{B}_{\mathrm{Re}}$ and $\mathbf{B}_{\mathrm{Im}}$ are real matrices. Since $\mathbf{B}$ is Hermitian, $\mathbf{B}_{\mathrm{Re}}$ is symmetric and $\mathbf{B}_{\mathrm{Im}}$ antisymmetric, i.e.,

$$\mathbf{B}^T = \mathbf{B}_{\mathrm{Re}} - i\mathbf{B}_{\mathrm{Im}}. \tag{22}$$

The matrix elements in both $\mathbf{B}_{\mathrm{Re}}$ and $\mathbf{B}_{\mathrm{Im}}$ will be built from terms which, when the matrix representation of the rotated operator is constructed, are multiplied with $\exp(ni\theta)$, where n is a positive or negative integer given by the r-dependence of each term. For example, in the matrix representation of the Hamiltonian in Eq. (2) the kinetic energy terms are multiplied with $\exp(-2i\theta)$ and the potential energy terms with $\exp(-i\theta)$. This will make the matrices $\mathbf{B}_{\mathrm{Re}}$ and $\mathbf{B}_{\mathrm{Im}}$ complex, but they will still be symmetric, respectively, antisymmetric, with respect to transposition, i.e.,

$$(\mathbf{B}^\theta)^T = \mathbf{B}_{\mathrm{Re}}^\theta - i\mathbf{B}_{\mathrm{Im}}^\theta. \tag{23}$$

We now return to the question of how a left eigenvector to a matrix relates to the corresponding right eigenvector. According to the definition, a left eigenvector to a matrix $\mathbf{B}$ is a row vector, $\mathbf{L}$, that fulfills

$$\mathbf{L}\mathbf{B} = \lambda\mathbf{L}. \tag{24}$$

When the transpose is taken of both the left- and the right-hand side of Eq. (24) it reads

$$(\mathbf{L}\mathbf{B})^T = \lambda\mathbf{L}^T$$

$$\Leftrightarrow$$

$$\mathbf{B}^T\mathbf{L}^T = \lambda\mathbf{L}^T. \tag{25}$$

Before proceeding we note that if $\mathbf{B}$ is symmetric, $\mathbf{B}^T = \mathbf{B}$, Eq. (25) is identical to the corresponding right eigenvalue

equation and thus $\mathbf{L}^T = \mathbf{R}$. If we further take the complex conjugate of Eq. (25), we get

$$\mathbf{B}^{T*}\mathbf{L}^{T*} = \lambda^*\mathbf{L}^{T*}$$

$$\Leftrightarrow$$

$$\mathbf{B}^\dagger\mathbf{L}^\dagger = \lambda^*\mathbf{L}^\dagger. \tag{26}$$

We see that if $\mathbf{B}$ is Hermitian, i.e., $\mathbf{B}^\dagger = \mathbf{B}$, λ is real and Eq. (26) is identical to the corresponding right eigenvalue equation, and consequently $\mathbf{L}^\dagger = \mathbf{R}$. For the matrix in Eq. (23), which has the symmetry of the matrix representation of the rotated Hamiltonian, we have

$$(\mathbf{B}^\theta)^\dagger = (\mathbf{B}_{\mathrm{Re}}^\theta)^* + i(\mathbf{B}_{\mathrm{Im}}^\theta)^*. \tag{27}$$

Since all the complexity in the matrices $\mathbf{B}_{\mathrm{Re}}$ and $\mathbf{B}_{\mathrm{Im}}$ comes from the factors $\exp(ni\theta)$ introduced through complex rotation, complex conjugation simply means that $\exp(ni\theta) \rightarrow \exp(-ni\theta)$, which identically gives the matrix representation of the operator rotated with $-\theta$, i.e.,

$$(\mathbf{B}^\theta)^\dagger = \mathbf{B}_{\mathrm{Re}}^{-\theta} + i\mathbf{B}_{\mathrm{Im}}^{-\theta} = \mathbf{B}^{-\theta}. \tag{28}$$

From Eq. (26) it now follows that

$$(\mathbf{B}^\theta)^\dagger\mathbf{L}^\dagger = \lambda^*\mathbf{L}^\dagger,$$

$$\mathbf{B}^{-\theta}\mathbf{L}^\dagger = \lambda^*\mathbf{L}^\dagger, \tag{29}$$

and we can conclude that the left eigenvectors of the matrix after rotation with θ are the complex conjugated transpose of the right eigenvectors to the matrix after rotation with $-\theta$,

$$\mathbf{L}^\theta = (\mathbf{R}^{-\theta})^\dagger, \tag{30}$$

where the eigenvalue associated with $\mathbf{R}^{-\theta}$ is λ^* if that associated with $\mathbf{L}^\theta$ is λ. Equation (30) is valid for left eigenvectors to all matrices, symmetric or not, produced by complex rotation of an initially Hermitian matrix. It is further consistent with the expression in Eq. (15). The ordinary Hermitian formulation is found as the special case when $\theta = 0$.

B. Time development

We now consider the time development, which is governed by the Schrödinger equation,

$$i\hbar\frac{\partial}{\partial t}\Psi(\mathbf{r},t) = H\Psi(\mathbf{r},t). \tag{31}$$

The rotation operator can again be used to obtain the corresponding complex rotated equation,

$$e^{\hat{A}}i\hbar\frac{\partial}{\partial t}\Psi(\mathbf{r},t) = e^{\hat{A}}He^{-\hat{A}}e^{\hat{A}}\Psi(\mathbf{r},t)$$

$$\Leftrightarrow$$

$$i\hbar\frac{\partial}{\partial t}\Psi^\theta(\mathbf{r},t) = H^\theta\Psi^\theta(\mathbf{r},t), \tag{32}$$

where $\Psi^\theta = \Psi(\mathbf{r}e^{i\theta},t)$. When the Hamiltonian, H, is time-independent, eigenstates to it multiplied with $\exp(-iE_nt/\hbar)$,

where E_n is the corresponding eigenenergy, will be solutions to Eq. (31). The time evolution of a wave function that is not an eigenstate to H can be found by expanding it in eigenstates. In a practical calculation this expansion will be made not in eigenstates to the true Hamiltonian H but in eigenstates to the matrix representation of it. In the case of complex rotation the pseudocontinuum eigenstates to the matrix representation, $\mathbb{H}^\theta$, will have complex eigenenergies, as in Eq. (20). As a consequence the exponent in the time-dependent part, $\exp(-iE_n t/\hbar)$, will no longer be purely imaginary, and the magnitude of the time-dependent function will, if $\theta > 0$, decrease exponentially when t increases. A rotated wave packet traveling out from the origin will thus be strongly suppressed before it reaches the boundary of the space used for its description. A rotation with $\theta < 0$ will consequently result in the opposite behavior. Which consequences does this have? Can we use the time-propagated complex rotated wave function to obtain physical information about our system? One approach to try and answer these questions is naturally to rotate back the complex rotated wave function to recover the unrotated one. If this is possible, all information should be available. In principle such a back rotation can be done either by the variable transformation $r \rightarrow r \exp(-i\theta)$ or by invoking $\exp(-\hat{A})$. We have studied both these approaches in practice and they are discussed in Sec. IV. Another possibility is to follow the procedure indicated by the expression in Eq. (15). The identity between the expressions in Eqs. (12) and (15) holds at each instant in time, as long as the wave function $\Psi(\mathbf{r},t)$ is well-represented in the space we use to describe it. The original (time-independent) norm can thus, at any time t, be recovered from the integral between the time propagated wave function rotated with θ and the complex conjugated corresponding function rotated with $-\theta$;

$$\int \Psi^*(\mathbf{r},t)\Psi(\mathbf{r},t)dV = \int [\Psi^{-\theta}(\mathbf{r},t)]^*\Psi^\theta(\mathbf{r},t)e^{3i\theta}dV. \tag{33}$$

The norm calculated as on the right-hand side of Eq. (33) is clearly *identical* to the norm in the Hermitian formulation, in spite of the fact that the integrands themselves are not identical. The norm is calculated with the so-called *c product*, which in Ref. [51] is dismissed due to what is called the "time-asymmetry problem." Although a calculation as on the right-hand side of Eq. (33) presents complications, we want to emphasize that it is formally correct. The challenge for the calculation is to preserve enough information in the time propagated states Ψ^θ (exponentially decreasing) and $\Psi^{-\theta}$ (exponentially increasing) that the integrand on the right-hand side of Eq. (33) remains finite. For long enough times the numerical accuracy required during the time-propagation will eventually grow beyond what is practically achievable, although it might be possible for a limited time. With the Floquet formalism, where the wave function at any time, t, is obtainable from the eigenstates to the *time-independent* Floquet matrix, the situation is radically different. Here it is possible to directly construct the integrand on the right-hand side of Eq. (33). This promising result for practical calcula-

tions of the *c product* will be further discussed in Sec. III C. A related issue is that of the correct calculation of expectation values. The same argument as for the norm can be applied to a matrix element of a general operator $\hat{O}$ taken between states for which the restricted space is adequate. Application of the operator $\exp(\hat{A})$ as before gives

$$\int \Psi_a^*(\mathbf{r},t)\hat{O}\Psi_b(\mathbf{r},t)dV = \int \Psi_a^*(\mathbf{r},t)e^{-\hat{A}}e^{\hat{A}}\hat{O}e^{-\hat{A}}e^{\hat{A}}\Psi_b(\mathbf{r},t)dV$$

$$\Leftrightarrow$$

$$\int \Psi_a^*(\mathbf{r},t)\hat{O}\Psi_b(\mathbf{r},t)dV = \int [\Psi_a^{-\theta}(\mathbf{r},t)]^*e^{\hat{A}}\hat{O}e^{-\hat{A}}\Psi_b^\theta(\mathbf{r},t)e^{3i\theta}dV$$

$$\Leftrightarrow$$

$$\int \Psi_a^*(\mathbf{r},t)\hat{O}\Psi_b(\mathbf{r},t)dV = \int [\Psi_a^{-\theta}(\mathbf{r},t)]^*\hat{O}^\theta\Psi_b^\theta(\mathbf{r},t)e^{3i\theta}dV, \tag{34}$$

where $\hat{O}^\theta = \hat{O}(r \rightarrow re^{i\theta})$, cf. Eq. (7). We conclude, in contrast to what is stated in Ref. [51], that the so-called *c product* will for bound states and physical wave packets give the same result as a Hermitian formulation for expectation values of any operator which is possible to rotate with the rotation operator, i.e., all operators which can be written as a sum of operators $\mathbf{r}^n$ and $\mathbf{p}^n$.

With many schemes for time-propagation neither the procedure to propagate both $\Psi^{-\theta}$ and Ψ^θ, nor the back rotation of the complex rotated solution will be practical due to the numerical limitations. It is thus important to establish what information we can get from Ψ^θ alone. Consider the wave function

$$\Psi(\mathbf{r},t) = \sum_n d_n(t)\Phi_n(\mathbf{r}), \tag{35}$$

where each Φ_n is an eigenstate with energy E_n to a matrix representation of a time-independent Hamiltonian H_0. The set of Φ_n's thus span the restricted space to which we limit our calculation. If also the full Hamiltonian is time-independent, the time-dependence of $d_n(t)$ is, as mentioned above, readily obtained from the Schrödinger equation, Eq. (31). We choose to keep that part separate and write

$$\Psi(\mathbf{r},t) = \sum_n e^{-iE_n t/\hbar}c_n(t)\Phi_n(\mathbf{r}). \tag{36}$$

Assuming that the restricted space is adequate to describe $\Psi(\mathbf{r},t)$, it can then be complex rotated by application of $\exp(\hat{A})$,

$$e^{i3\theta/2}\Psi^\theta(\mathbf{r},t) = e^{\hat{A}}\Psi(\mathbf{r},t) = e^{\hat{A}}\sum_n d_n(t)\Phi_n(\mathbf{r}). \tag{37}$$

The rotated wave function can also be expressed in eigenstates to H_0^θ, the time-independent part of the *complex rotated* Hamiltonian,

$$\Psi^\theta(\mathbf{r},t) = \sum_n d_n^\theta(t)\Phi_n^\theta(\mathbf{r}) = \sum_n e^{-iE_n^\theta t/\hbar}c_n^\theta(t)\Phi_n^\theta(\mathbf{r}). \quad (38)$$

Thus

$$e^{\hat{A}}\sum_n d_n(t)\Phi_n(\mathbf{r}) = e^{i3\theta/2}\sum_n d_n^\theta(t)\Phi_n^\theta(\mathbf{r}). \quad (39)$$

Note that generally $\exp(i3\theta/2)\Phi_n^\theta(\mathbf{r}) \neq \exp(\hat{A})\Phi_n(\mathbf{r})$ since most of the states $\Phi_n(\mathbf{r})$ will be eigenstates only to the matrix representation of the Hamiltonian. If now a specific $\Phi_n(\mathbf{r})$ is an eigenstate to the true Hamiltonian, and not only to a matrix representation of it, then indeed

$$e^{\hat{A}}\Phi_n(\mathbf{r}) = e^{i3\theta/2}\Phi_n^\theta(\mathbf{r}) \quad (40)$$

and consequently the coefficients $d_n^\theta(t)$ in Eq. (38) and $d_n(t)$ in Eq. (35) are equal. Furthermore, in this case E_n^θ will be real and equal to $E_n^{\theta=0}$, and thus also c_n^θ in Eq. (38) and c_n in Eq. (36) are equal. The same conclusion was also reached by Scrinzi and Piraux [46]. The population of any bound state, well-represented in the finite space addressed by the calculation, can thus be calculated as $|d_n^\theta|^2 = |c_n^\theta|^2$.

Consider now a general wave function $\Psi(\mathbf{r},t)$, e.g., representing an atomic state after exposure to a laser pulse, described in a restricted but adequate space. The complex rotated counterpart, $\Psi^\theta(\mathbf{r},t)$, will be a superposition of eigenstates Φ_n^θ to a matrix representation of the complex rotated Hamiltonian. This superposition may represent the situation discussed above; a state that is a mixture of a bound part and a wave packet traveling out from the atom. The eigenstates building up the wave packet will in general have complex energies. The magnitude of the coefficients d_n^θ in Eq. (38) will, when E_n is complex, decrease exponentially with time. The sum of the absolute squares of the d_n^θ's will therefore after sufficient time approach the sum of the absolute squares of coefficients of the bound part of the wave function, or more precisely the bound part of the wave function that is adequately described in the restricted space, i.e., it will approach the survival probability,

$$\sum_n |d_n^\theta(t)|^2 \xrightarrow{t\to\infty} \sum_{i=\text{bound}} |d_n^\theta|^2 = \sum_{i=\text{bound}} |c_n^\theta|^2. \quad (41)$$

We have thus found that if the time-dependent Schrödinger equation is solved with complex rotation, the coefficient preceding each bound state is identical to what would be found in a Hermitian calculation, and thus its absolute squared value can still be interpreted as the probability to find the system in that particular state. Furthermore, after some inter-

action, the sum of the absolute squares of *all* coefficients, preceding bound as well as pseudocontinuum states will approach the survival probability of the system as time increases. This statement also holds when resonances are present. Important information about the process at hand can thus be obtained from the time-propagation of $\Psi^\theta(\mathbf{r},t)$ only.

Finally we want to discuss one physically interesting quantity that cannot be obtained with $\Psi^\theta(\mathbf{r},t)$ alone, the photoelectron spectrum. To obtain it we see at least two possibilities. The first is to back-rotate $\Psi^\theta(\mathbf{r},t)$ to obtain $\Psi(\mathbf{r},t)$. How this is done in practice will be described in Sec. V B. The second possibility is to utilize the decomposition in Eq. (38) and the fact that the *c product* norm, the right-hand side of Eq. (33), is time-independent. Assuming a normalized wave function at $t=0$ we have

$$\int [\Psi^{-\theta}(\mathbf{r},t)]^*\Psi^\theta(\mathbf{r},t)e^{3i\theta}dV$$

$$= \sum_{m,n} \int [d_m^{-\theta}(t)\Phi_m^{-\theta}(\mathbf{r})]^*d_n^\theta(t)\Phi_n^\theta(\mathbf{r})e^{3i\theta}dV$$

$$= \sum_n [d_n^{-\theta}(t)]^*d_n^\theta(t) = 1. \quad (42)$$

For the bound states in the sum over n, each term $[d_n^{-\theta}(t)]^*d_n^\theta(t)$ gives the probability to find the electron in that state. For the part of the electron spectrum that lies in the continuum, the ionization probability per energy interval, $dP_\text{ion}/d\varepsilon$, can be extracted through

$$\frac{dP_\text{ion}}{d\varepsilon} = \frac{1}{\pi} \text{Im}\left(\sum_n \frac{[d_n^{-\theta}(t)]^*d_n^\theta(t)}{E_n^\theta - \varepsilon} \right), \quad (43)$$

where ε is the continuum energy and E_n^θ is the (generally complex) eigenvalue associated with $\Phi_n^\theta(\mathbf{r})$. The sum over n runs over the whole spectrum since each pseudocontinuum state contributes over a wide range of energies, see further the discussion in Sec. V. The above relation is analogous to the optical theorem. By considering the Hermitian expectation value of the Green's operator, $\hat{G}(\varepsilon)=1/(H-\varepsilon)$, it is found that $\text{Im}\langle\Psi|\hat{G}(\varepsilon)|\Psi\rangle = \pi|\langle\psi_\varepsilon|\Psi\rangle|^2 = \pi dP_\text{ion}/d\varepsilon$, see, e.g., Ref. [13]. As previously discussed, expectation values calculated with rotated wave functions and operators using the *c* product should reproduce the corresponding Hermitian result. Hence the expectation value may be calculated using the rotated wave function and the rotated Green's operator $\hat{G}^\theta(\varepsilon)$ instead of the Hermitian representation. By applying the closure relation we find that

$$\pi\frac{dP_\text{ion}}{d\varepsilon} = \text{Im}\left(\sum_n \frac{\int [\Psi^{-\theta}(\mathbf{r})]^*\Phi_n(\mathbf{r})e^{3i\theta}dV \int [\Phi^{-\theta}(\mathbf{r}')]^*\Psi^\theta(\mathbf{r}')e^{3i\theta}dV'}{E_n^\theta - \varepsilon} \right), \quad (44)$$

which is equivalent to Eq. (43). Calculations using both Eq. (43) and the back-rotated wave function are presented in Sec. V.

III. METHOD

In the following we will be concerned with the solution of the time-dependent Schrödinger equation, Eq. (31), where the time-development is governed by the Hamiltonian H,

$$H = H_0 + H_I, \tag{45}$$

with H_0 being the time-independent part, e.g., for a one-particle system

$$H_0 = \frac{\mathbf{p}^2}{2m} - \frac{Ze^2}{4\pi\varepsilon_0 r}, \tag{46}$$

and H_I an explicitly time-dependent perturbation from a light pulse. The interaction between an electron and the light pulse is in the velocity gauge given by

$$H_I = \frac{e}{m}\mathbf{p} \cdot \mathbf{A}(t). \tag{47}$$

We work here in the dipole approximation and do not consider any spatial dependence in the vector potential $\mathbf{A}$. We assume linearly polarized light and consider in most cases $\sin^2$-shaped envelopes

$$\mathbf{A}(t) = A_0 \sin(\omega t + \varphi)\sin^2(\pi t/T)\hat{\mathbf{z}}, \tag{48}$$

where T is the pulse duration. Also the length gauge version of H_I,

$$H_I = -e\mathbf{r} \cdot \frac{\partial \mathbf{A}(t)}{\partial t}, \tag{49}$$

has been used to check for gauge invariance, but all the presented examples are calculated in the velocity gauge. Our prime interest is to investigate advantages and possible problems with complex rotation. As discussed in Sec. II, this rotation is performed by the transformation $\mathbf{r} \rightarrow \mathbf{r}e^{i\theta}$, which also implies that $\mathbf{p} \rightarrow \mathbf{p}e^{-i\theta}$.

To obtain a complete and finite basis set well-suited to solve the Schrödinger equation, Eq. (31), we use so-called B splines, see, e.g., Ref. [57]. The use of B splines in atomic physics was pioneered by Johnson and Sapirstein [58] 20 years ago and later it has been the method of choice in a large number of studies, as reviewed, e.g., in Ref. [59]. B splines are piecewise polynomials of a chosen order k defined on a so-called knot sequence, and they form a complete set in the space defined by the knot sequence and the B spline order [57]. If N is the number of knots there are $N-k$ B splines in the set. The radial part of the eigenstates to the Hamiltonian, $R_{n,\ell}$, is expanded in B splines

$$rR_{n,\ell}(r) = P_{n,\ell}(r) = \sum_{i=2}^{N-k-1} \xi_i B_i(r), \tag{50}$$

where the first and last B spline have been removed. Hereby the boundary conditions that $P_{n,\ell}(r=0)=0$ and $P_{n,\ell}(r=R)$

$=0$ are imposed. Typically 40–70 points are used in the knot sequence, distributed either linearly throughout the domain or linearly in the inner region and then exponentially further out. The last knot, defining the box to which we limit our problem, is in most cases around 100 Bohr radii and the polynomial order k is seven. The coefficients ξ_i in Eq. (50) are found by diagonalization of the matrix

$$\mathbb{H}^\theta \xi = \epsilon \mathbf{B} \xi, \tag{51}$$

where

$$\mathbb{H}^\theta_{ij} = \int B_i(r)Y^*_{\ell m}(\Omega)H(\mathbf{r}e^{i\theta})B_j(r)Y_{\ell'm'}(\Omega)dV \tag{52}$$

and

$$B_{ij} = \int B_i(r)B_j(r)dr. \tag{53}$$

Equation (51) is a generalized eigenvalue problem that can be solved with standard numerical routines. The angular parts of the eigenstates are given by the spherical harmonics, $Y_{\ell m}$, and for each angular symmetry we get $N-k-2$ eigenstates. For the lower energy eigenstates the box and the knot sequence provide an adequate description of the real physical space. For these states we find the solution to the true physical Hamiltonian. The higher energy eigenstates are determined mainly by the box. They are thus unphysical, but still essential for the completeness of the basis set. As discussed in connection with the relation in Eq. (20), the energy of the latter will be complex.

For the solution to the Schrödinger equation, Eq. (31), we have investigated three different procedures. Two of the methods solve the problem on a time grid. With the first method, Sec. III A, we work with eigenstates to H_0^θ, i.e., $H^\theta=H_0^\theta$ in Eq. (51), and $H_I^\theta(t)$ is treated as a perturbation. With the second method, Sec. III B, we use eigenstates to $H_0^\theta+H_I^\theta(t_i)$ for each time interval, i.e., it is an expansion in field dressed basis sets. The third method, Sec. III C, is an implementation of the Floquet formalism. Here eigenstates to the unperturbed Hamiltonian, H_0^θ, are used to expand the spatial part of the eigenstates to the time-dependent Floquet Hamiltonian.

A. Time propagation in eigenstates to the unperturbed Hamiltonian

Consider the expansion of $\Psi^\theta(\mathbf{r},t)$, Eq. (38), in eigenstates, Φ_n^θ, to the time-independent Hamiltonian H_0^θ. To first order in time the coefficients $c_i^\theta(t)$ obey

$$c_i^\theta(t + \Delta t) = c_i^\theta(t) + \Delta t \dot{c}_i^\theta(t). \tag{54}$$

Insertion of Eq. (38) into the Schrödinger equation, Eq. (31), then gives

$$\dot{c}_i^\theta(t) = -\frac{i}{\hbar} \sum_j c_j^\theta(t) e^{-i(E_j^\theta - E_i^\theta)t/\hbar}$$

$$\times \int [\Phi_i^{-\theta}(\mathbf{r})]^* H_I^\theta(\mathbf{r},t) \Phi_j^\theta(\mathbf{r}) e^{3i\theta} dV. \quad (55)$$

Hence Eqs. (54) and (55) allow a stepwise evaluation of Ψ^θ in time. The efficiency of this method is improved considerably with some higher order Runge-Kutta scheme that can provide a better estimate of $c_i^\theta(t+\Delta t)$ by weighting several $\dot{c}_i^\theta$ at different times. The scheme used here is a fifth order Runge-Kutta method with Cash-Karp coefficients [60]. This scheme has also the advantage that it allows a simple error analysis, which here is explored in an adaptive step-size control. We have further found that calculation of $\dot{c}_i^\theta(t)\exp[-iE_i(t+\Delta t)/\hbar]$ and storage of $c_i^\theta(t)\exp(-iE_i t/\hbar)$ is numerically more stable than calculation of $\dot{c}_i^\theta(t)$ and storage of $c_i^\theta(t)$. This is due to numerical difficulties in the calculation of $\exp[-i(E_j^\theta - E_i^\theta)t/\hbar]$ with complex eigenenergies.

B. Expansion in field dressed basis sets

Another possibility is to find the eigenfunctions to $H(t_i)$ for each t_i. Between the time-points the system is allowed to develop according to $H(t_i)$. At the next point in the time grid the system is just projected onto the solutions of $H(t_{i+1})$. Assuming the solutions to the full Hamiltonian to be known at the time t_i, i.e.,

$$H^\theta(t_i)|\chi_i^{n,R}\rangle = E_i^n|\chi_i^{n,R}\rangle, \quad (56)$$

a state that is in a superposition of solutions to $H^\theta(t_i)$ will develop in time as

$$|\Psi(t_i)\rangle = \sum_n c_n^i|\chi_i^{n,R}\rangle \Rightarrow |\Psi(t_i + \Delta t)\rangle = \sum_n c_n^i|\chi_i^{n,R}\rangle e^{-iE_i^n\Delta t}$$

$$(57)$$

and can then be projected onto solutions to $H(t_{i+1})$. For this we need the closure relation

$$\sum_n |\chi_{i+1}^{n,R}\rangle\langle\chi_{i+1}^{n,L}| = 1, \quad (58)$$

where the labels R and L denote the right and left eigenvector to the Hamiltonian, $H(t_{i+1})$, as discussed in Sec. II A. There is an important difference between the Hamiltonian expressed in the length, respectively, velocity gauge when complex rotation is used. The matrix representation of the field free Hamiltonian is symmetric. If the interaction with the electromagnetic field is expressed in the length gauge, this symmetry is preserved and the left eigenvectors are just the transposes of the right eigenvectors, cf. Eq. (25). When the interaction with the electromagnetic field is expressed in the velocity gauge, on the other hand, the Hamiltonian will be of the general form of Eq. (21), and the left eigenvectors are distinctly different from the right eigenvectors. However, standard numerical routines provide right as well as left eigenvectors, and we can easily construct $\Psi(t_{i+1})$ in the new basis

$$|\Psi(t_{i+1})\rangle = \sum_n |\chi_{i+1}^{n,R}\rangle\langle\chi_{i+1}^{n,L}|\Psi(t_i + \Delta t)\rangle = \sum_n c_n^{i+1}|\chi_{i+1}^{n,R}\rangle.$$

$$(59)$$

The procedure is then repeated from Eq. (57) to obtain the wave function at the next time step. Compared to the method outlined in Sec. III A, substantially fewer time points are needed. On the other hand, the Hamiltonian has to be rediagonalized at every time step.

C. Floquet theory

The third and last method investigated in this work is based on Floquet's theorem [61]. We follow the formulation proposed by Shirley [29] and truncate an infinite-dimensional, time-independent matrix representation of the Floquet Hamiltonian, $\mathbb{H}_F$. The quantum state vector is then retrieved, at any finite time t, from the eigenstates and eigenvalues of $\mathbb{H}_F$. However, we differ from Shirley's formulation in that we examine the application of Floquet's theorem to quantum systems in the context of complex rotation. Combining complex rotation with Floquet theory means specifically that we consider a non-Hermitian matrix $\mathbb{H}_F^\theta$. The Hermitian description can be recovered with $\theta = 0$. Although the combination of Floquet theory and complex rotation has been used before, see, e.g., Ref. [32] and references therein, we repeat the basic steps here in order to be able to discuss the time propagation of wave functions.

For Hamiltonians periodic in time, $H^\theta(t+2\pi/\omega) = H^\theta(t)$, we may make use of Floquet's theorem and express the associated state vector as

$$\Psi^\theta(\mathbf{r},t) = \sum_j a_j^\theta e^{-i\epsilon_j^\theta t/\hbar}\chi_j^\theta(\mathbf{r},t) \quad (60)$$

with the constants a_j^θ given by

$$a_j^\theta = \int [\chi_j^{-\theta}(\mathbf{r},0)]^*\Psi^\theta(\mathbf{r},0)e^{3i\theta}dV. \quad (61)$$

The χ_j^θ states are obtained, along with the quasienergies ϵ_j^θ, from

$$\left(H^\theta - i\hbar\frac{\partial}{\partial t}\right)\chi_j^\theta(\mathbf{r},t) = \epsilon_j^\theta\chi_j^\theta(\mathbf{r},t). \quad (62)$$

Thus $\exp(-i\epsilon_j^\theta t/\hbar)\chi_j^\theta(\mathbf{r},t)$ are solutions to the complex rotated time-dependent Schrödinger equation, and consequently they form a complete basis set. Furthermore, the imaginary part of ϵ_j^θ gives the half width of the field dressed state $\chi_j^\theta(\mathbf{r},t)$. The operator $H^\theta - i\hbar\partial_t$ is usually referred to as the Floquet Hamiltonian.

An important property of the solutions χ_j^θ, easily seen from Eq. (62), is that they evolve with the same periodicity in time as the Hamiltonian describing the system. The periodicity of χ_j^θ, as well as that of the Hamiltonian, is frequently used to expand both of them in complex Fourier series. The idea is thus to expand χ_j^θ in products of a spatial function, $\kappa_{j,k}^\theta(\mathbf{r})$, and a time-periodic function. Subsequently, the spatial functions are expanded in the box-normalized eigenstates, Φ_n^θ, to the unperturbed Hamiltonian H_0^θ,

$$\chi_j^\theta(\mathbf{r},t) = \sum_{k=-\infty}^{\infty} \eta_{j,k} e^{ik\omega t} \kappa_{j,k}^\theta(\mathbf{r}) = \sum_{k=-\infty}^{\infty} e^{ik\omega t} \sum_n b_{j,k}^{\theta,n} \Phi_n^\theta(\mathbf{r}).$$

(63)

If the χ_j^θ states, constructed using Eq. (63), are normalized at time $t=0$, they remain orthonormal to each other at later times, a property very convenient for an instantaneous basis in space. The full Hamiltonian is given in the velocity gauge for light linearly polarized along the z direction as

$$H^\theta = H_0^\theta + \frac{e}{m} \sum_{q=-\infty}^{\infty} A_q e^{iq\omega t} p_z e^{-i\theta}$$

(64)

with

$$A_q = \frac{\omega}{2\pi} \int_0^{2\pi/\omega} A(t) e^{-iq\omega t} dt.$$

(65)

For monochromatic light we have only two nonzero A_q's corresponding to $q=\pm 1$. If the expansion of Ψ^θ in the set of functions Φ_n^θ is known at time $t=0$, the expression for the coefficients a_j^θ in Eq. (61) can be given in a more convenient form. Comparing the general expansion of Ψ^θ, Eq. (38), in the unperturbed atomic states Φ_n^θ at $t=0$, with that of Eq. (60), i.e.,

$$\sum_n d_n^\theta(0) \Phi_n^\theta(\mathbf{r}) = \sum_j a_j^\theta \chi_j^\theta(\mathbf{r},0),$$

(66)

we find that

$$a_j^\theta = \sum_n d_n^\theta(0) \int [\chi_j^{-\theta}(\mathbf{r},0)]^* \Phi_n^\theta(\mathbf{r}) e^{3i\theta} dV$$

$$= \sum_n d_n^\theta(0) \sum_{k=-\infty}^{\infty} (b_{j,k}^{-\theta,n})^*,$$

(67)

where the expansion in Eq. (63) and the orthonormality of the basis $\Phi_n^\theta(\mathbf{r})$ are used in the last step. Finally, combining Eqs. (60), (63), and (67) we find the expression for $d_n^\theta(t)$ as

$$d_n^\theta(t) = \sum_j \left(\sum_{n'} d_{n'}^\theta(0) \sum_{k'=-\infty}^{\infty} (b_{j,k'}^{-\theta,n'})^* \right) e^{-i\epsilon_j^\theta t/\hbar} \sum_{k=-\infty}^{\infty} e^{ik\omega t} b_{j,k}^{\theta,n}.$$

(68)

The sum over j in Eq. (68) will in practice run over a finite number of N_χ states. This number, N_χ, is furthermore identical to the number of included basis states, $\Phi_n^\theta(\mathbf{r})$. The number of B splines, discussed in connection with Eq. (50), along with the number of partial waves is therefore what determines the number of basis states χ_j^θ.

For a wave function rotated in the opposite direction,

$$\Psi^{-\theta}(\mathbf{r},t) = \sum_n d_n^{-\theta}(t) \Phi_n^{-\theta}(\mathbf{r}),$$

(69)

the expression corresponding to Eq. (68) is given by

$$d_n^{-\theta}(t) = \sum_j \left(\sum_{n'} d_{n'}^{-\theta}(0) \sum_{k'=-\infty}^{\infty} (b_{j,k'}^{\theta,n'})^* \right) e^{-i(\epsilon_j^\theta)^* t/\hbar} \sum_{k=-\infty}^{\infty} e^{ik\omega t} b_{j,k}^{-\theta,n}.$$

(70)

In Eq. (70) the relation $\epsilon_j^{-\theta} = (\epsilon_j^\theta)^*$ is used, analogous to what is discussed in connection with Eq. (30).

Combining Eq. (68) and Eq. (70) gives

$$[d_n^{-\theta}(t)]^* d_n^\theta(t) = \sum_{j,j'} (a_{j'}^{-\theta})^* a_j^\theta e^{-i(\epsilon_j^\theta - \epsilon_{j'}^\theta) t/\hbar}$$

$$\times \sum_{k,k'=-\infty}^{\infty} e^{i(k-k')\omega t} b_{j,k}^{\theta,n} (b_{j',k'}^{-\theta,n})^*$$

(71)

with

$$(a_{j'}^{-\theta})^* a_j^\theta = \left(\sum_{n'} [d_{n'}^\theta(0)]^* \sum_{k'=-\infty}^{\infty} b_{j',k'}^{\theta,n'} \right)$$

$$\times \left(\sum_n d_n^\theta(0) \sum_{k=-\infty}^{\infty} (b_{j,k}^{-\theta,n})^* \right).$$

(72)

In disagreement with Buchleitner and co-workers, see Eq. (36) of Ref. [49], we argue that $\epsilon_{j'}^\theta$ in Eq. (71) is *not* to be complex conjugated. For bound states, as discussed in connection with Eq. (42), $[d_n^{-\theta}(t)]^* d_n^\theta(t)$ gives the probability of the system to be in the particular state Φ_n^θ. We want to emphasize that a numerically more stable approach to finding this probability is to follow the procedure indicated in Eq. (41) and compute $|d_n^\theta|^2$ using Eq. (68). For unbound states, however, $d_n^{-\theta}$ is not given from d_n^θ and a general expression such as Eq. (71) is required. Unlike the corresponding expressions obtained with the methods in Secs. III A and III B, in which we would have to evaluate $\Psi^{-\theta}$ and Ψ^θ separately and stepwise in time, the convenient form of Eq. (71) allows a simple numerical analysis of $[d_n^{-\theta}(t)]^* d_n^\theta(t)$. We notice first that as long as the sums over j and j' run over a finite number of states, $[d_n^{-\theta}(t)]^* d_n^\theta(t)$ will eventually diverge because of the imaginary parts of ϵ_j^θ and $\epsilon_{j'}^\theta$. However, for moderate times, convergent results are obtainable with Eq. (71). A higher density of pseudocontinuum states in the imaginary region of ϵ_j^θ, made possible by choosing a larger box and/or a smaller scaling angle θ, will suppress this divergence and thus prolong the applicability of Eq. (71). In practice, however, since any numerical error is blown up by the exponential factor, the divergence will generally occur earlier than expected. The numerical error is, if larger than machine accuracy, usually caused by the early truncation of k in Eq. (63) necessary to keep the size of $\mathbb{H}_F^\theta$ down, as will be discussed shortly. To reduce this error a cut in $\mathrm{Im}(\epsilon_j^\theta - \epsilon_{j'}^\theta)$ is introduced. It is important that with this cut the largest allowed exponent is large enough to include all the significant terms in Eq. (71) but still small enough to suppress the terms that blow up due to numerical limitations. Also it is important that the truncation of k is such that significant terms associated with large exponential factors are accurately computed. Checking whether Eq. (42) holds offers a possible test

for accuracy. Finally we want to point out that expectation values should in principle be possible to compute using this technique as discussed in Sec. II B.

We will now focus on how ϵ_j^θ, $b_{j,k}^{\theta,n}$, and $b_{j,k}^{-\theta,n}$ are computed in practice. By introducing Eqs. (63) and (64) in Eq. (62) we obtain an infinite set of coupled equations:

$$
\sum_{n'} \sum_{k'=-\infty}^{\infty} \left[(E_{n'}^\theta + k'\hbar\omega)\delta_{n'n}\delta_{k'k} \right.
$$
$$
\left. + \frac{e}{m} A_{k-k'} \int [\Phi_n^{-\theta}(\mathbf{r})]^* p_z e^{-i\theta} \Phi_{n'}^\theta(\mathbf{r}) e^{3i\theta} dV \right] b_{j,k'}^{\theta,n'} = \epsilon_j^\theta b_{j,k}^{\theta,n},
$$
(73)

where E_n^θ is the eigenvalue associated with Φ_n^θ. An approximate solution to Eq. (73) is obtained through truncation of k, $-k_m \leq k \leq k_m$, in the Fourier expansion of χ_j^θ. This truncated version of Eq. (73) is easily transformed to a matrix representation as a $(2k_m+1)N_\chi$-dimensional matrix, $\mathbb{H}_F^\theta$. The quantities ϵ_j^θ and $b_{j,k}^{\theta,n}$ are subsequently obtained as eigenvalues and individual elements of the corresponding right eigenvectors. The $(b_{j,k}^{-\theta,n})^*$'s are, as described in Sec. II A, found as elements of the left eigenvectors. A set of $2(k_m+1)N_\chi$ states χ_j^θ is generated in this procedure. However, as indicated earlier, only N_χ of these states are required in Eq. (68). The reason why not all states are included in Eq. (68) is that several states obtained from the diagonalization of the Floquet Hamiltonian represent the same solution $\exp(-i\epsilon_j^\theta t/\hbar)\chi_j^\theta$. This redundancy is seen from the following transformation:

$$
\epsilon_j \rightarrow \epsilon_j + m_j\hbar\omega, \tag{74}
$$

$$
\chi_j^\theta(\mathbf{r},t) \rightarrow e^{im_j\omega t}\chi_j^\theta(\mathbf{r},t), \tag{75}
$$

with m_j being an integer number. Now, as easily verified, Eq. (62) remains satisfied after this transformation. Hence, both χ_j^θ and $\exp(im_j\omega t)\chi_j^\theta$ are eigenvectors to the truncated version of Eq. (73) with eigenvalues ϵ_j and $\epsilon_j+m_j\hbar\omega$, respectively. Although they represent the same solution to the rotated time-dependent Schrödinger equation, a subtle difference exists between the two states. This difference is caused by the imposed truncation of k,

$$
e^{-i\epsilon_j^\theta t/\hbar}\chi_j^\theta(\mathbf{r},t) = e^{-i\epsilon_j^\theta t/\hbar} \sum_{k=-\infty}^{\infty} e^{ik\omega t} \sum_n b_{j,k}^{\theta,n} \Phi_n^\theta(\mathbf{r})
$$

$$
\Leftrightarrow
$$

$$
e^{-i(\epsilon_j^\theta + m_j\hbar\omega)t/\hbar} e^{im_j\omega t}\chi_j^\theta(\mathbf{r},t)
$$
$$
= e^{-i(\epsilon_j + m_j\hbar\omega)t/\hbar} \sum_{k'=-\infty}^{\infty} e^{ik'\omega t} \sum_n b_{j,k'-m_j}^{\theta,n} \Phi_n^\theta(\mathbf{r}), \quad (76)
$$

with $k'=k+m_j$. Hence as k and k' are truncated, the two formulations will use different sets of spatial functions $\kappa_{j,k}^\theta$.

The last part of this section will be devoted to the limitations of the method just described. One significant limitation is obviously that Floquet's theorem only applies to periodic

perturbations. This means specifically that atoms exposed to finite laser pulses cannot be treated within this formalism. Several modifications have, however, been suggested to evade this theoretical restriction. For pulses lasting a substantial number of optical cycles, one successful approach [62] is to express the electromagnetic field as

$$
\mathcal{E}(t)\hat{z} = E_0(t)\sin[\omega(t)t + \varphi(t)]\hat{z} \tag{77}
$$

and treat the amplitude $E_0(t)$, frequency $\omega(t)$, and phase $\varphi(t)$ as a slowly varying modulation on some periodic carrier wave. Another possible modification is the use of the many-mode Floquet theorem, as described by Ho and co-workers [63], for systems exposed to multicolor lasers with incommensurate frequencies. For $\sin^2$-shaped pulses with duration of only a few optical cycles we would like to introduce the possibility of yet another approach: If, instead of a single laser pulse, a train of identically shaped pulses perturbs the atom, the Hamiltonian becomes periodic in time. In this case, Eqs. (63) and (64) are adequate expressions if used with a period defined by the pulse length rather than the period of the carrier. Furthermore, if the single pulse consists of an integer number of optical cycles (as will be considered in this work), the Fourier expansion of **A**, Eq. (65), consists generally of only six nonzero A_q's. Now, the spatial independence of **A** (as assumed in the dipole approximation) implies that the interaction between the atom and the very first pulse in the infinite sequence of pulses is identical to that experienced between the atom and the single pulse in our original problem. However, if we were to examine the system at a finite time after its exposure to the first pulse, the two physical descriptions will obviously differ. Hence time has to be divided into two regions; one in which the atom is exposed to the single laser pulse and another in which it is not. In the first region propagation using Floquet theory, as described here, is applicable and in the second the field-free evolution of the atomic states has to be used. Alternatively, if the frequencies defined by the envelope and the carrier wave are incommensurate, a bicolor laser field could be generated by allowing for nonidentical pulses in the pulse train. The system could then be treated with the many-mode Floquet theorem. This alternative approach was earlier used by Huang and Chu [64]. A second limitation of the method just considered is that the Floquet matrix usually becomes extremely large in practice. However, only a fraction of the eigenstates and eigenvalues are required which improves the situation, see, e.g., the techniques used in Refs. [65,66]. Since we only consider hydrogen here, diagonalization of the entire matrix is still possible. Instead, we are faced with the difficulty of selecting a complete set of χ_j^θ out of all eigenvectors obtained from the diagonalization of $\mathbb{H}_F^\theta$. For the identification of a complete set the basic problem is that we lack knowledge of m_j, see Eqs. (74) and (75), for the different χ_j^θ-states obtained. However, this knowledge could be retrieved through the parameter

$$
x_j = \frac{\sum_k k \sum_n |(b_{j,k-m_j}^{-\theta,n})^* b_{j,k-m_j}^{\theta,n}|}{\sum_k \sum_n |(b_{j,k-m_j}^{-\theta,n})^* b_{j,k-m_j}^{\theta,n}|}. \tag{78}
$$

For infinite Fourier series, x_j will differ by m_j between two states with quasienergies ϵ_j and $\epsilon_j+m_j\hbar\omega$, respectively.
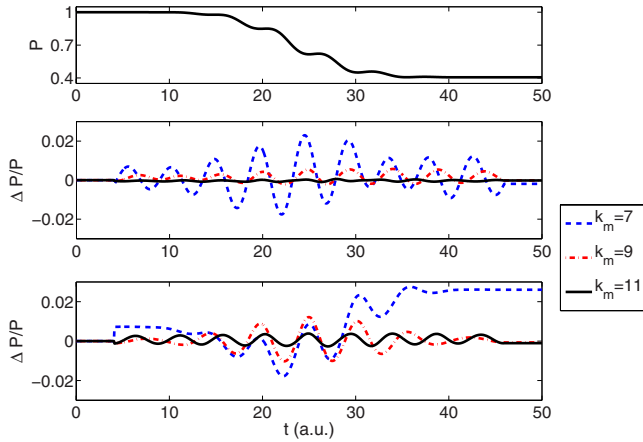
FIG. 1. (Color online) *Upper panel*: The population of the atomic ground state of hydrogen obtained using the method of Sec. III A. The atom is perturbed by a $\sin^2$-shaped pulse that has a peak intensity of 1.5×10^{15} W/cm^2, a central frequency of $\omega = 0.6$ a.u., and a duration corresponding to four optical cycles. The scaling angle θ is here 30°. *Middle panel*: The relative difference between the population of the ground state as calculated using Floquet theory, Eq. (68), and that obtained in the upper panel. Convergence is seen with increasing k_m, i.e., with increasing limit to the Fourier series expansion of $\chi_j(\mathbf{r}, t)$. A complete set of χ_j states is identified based on Eq. (78). *Lower panel*: Identical to the second panel except that the set of χ_j states is obtained by choosing those with $-\hbar\omega/2 \leqslant \mathrm{Re}(\epsilon_j) < \hbar\omega/2$.

Hence a complete set of χ_j^θ is obtained from choosing those with x_j in any interval of unity length. The truncation of k spoils this nice behavior. Nevertheless, the most converged eigenstates are likely to be located in an interval centered at $x_j = 0$. In practice, the interval could be expanded slightly to include a minimum of N_χ states before choosing those best satisfying the closure relation. Fortunately, however, for k_m large enough to accurately describe the dynamics of the system, N_χ states will generally be found having $-0.5 \leqslant x_j < 0.5$ and the later modification is not necessary. Thus in comparison (see Fig. 1) to the frequently used technique of excluding all states except those with real parts of ϵ_j located in some window of size $\hbar\omega$, this approach has two advantages. First, it always identifies a complete set of χ_j states, even for moderate values of k_m. Second, the states identified are likely to be the most accurately described.

IV. EXAMPLES

In the following we aim to illustrate some of the numerical advantages and challenges related to the application of uniform complex scaling to dynamical systems. We have demonstrated in Sec. II that all physical information obtainable with a Hermitian formalism may be obtained also with a complex rotated formalism. The drawback is that "left state" refers to the Hamiltonian $H^{-\theta}$, instead of H^θ, and propagation with $H^{-\theta}$ may not be very convenient. The following numerical examples will focus on the propagation of the "right state," Ψ^θ, only. In addition, to illustrate which numerical benefits that may be achieved with complex rotation, we will
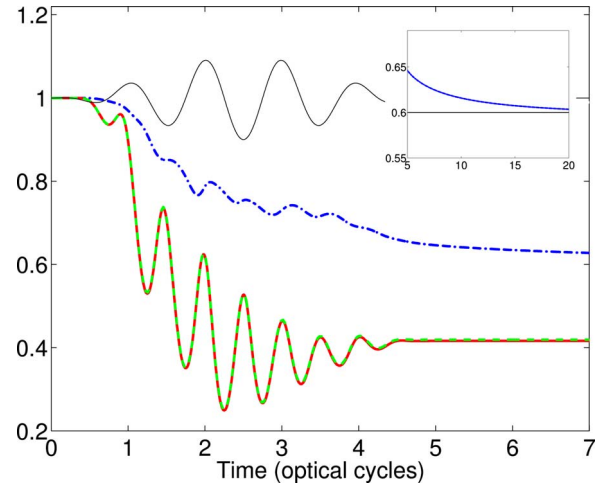

FIG. 2. (Color online) Population of the initial state and the sum of the absolute squares of the amplitudes as functions of time for a hydrogen atom initially in the ground state exposed to an oscillating electric field with a $\sin^2$-shaped envelope with a duration of five optical cycles. The maximum electric field strength is 10 a.u. (corresponding to a peak intensity of 3.5×10^{18} W/cm^2), and the central frequency is 2.0 a.u. (corresponding to a photon energy of about 54 eV). The thin black curve is the vector potential. The full (red) curve is the population of the initial state in the velocity gauge obtained as described in Sec. III A, which is checked to coincide with the solution according to the methods of Secs. III B and III C. The scaling angle θ is here 15°. The dashed (green) one is the same quantity obtained by numerical integration of the Hermitian Schrödinger equation on a grid. The dash-dotted (blue) curve is the sum $\Sigma_n |d_n^\theta(t)|^2$ where the d_n^θ's are the coefficients in an expansion of the rotated wave function in eigenstates of the unperturbed Hamiltonian, H_0^θ. The inset shows how this sum converges towards the probability of the system not being ionized, see the limit in Eq. (41).

also discuss to what extent physical information may be extracted from the rotated wave function.

We have argued, cf. Eq. (41), that the population of the nth bound state can be obtained as $|d_n^\theta(t)|^2$, which should be independent of θ as long as the allocated space is adequate. If the left eigenstates of the unperturbed Hamiltonian, $\Phi_n^{-\theta}$, are known, each $d_n^\theta(t)$ is found through the projection

$$d_n^\theta = \int_0^R [\Phi_n^{-\theta}(\mathbf{r})]^* \Psi^\theta(\mathbf{r}, t) e^{3i\theta} dV. \tag{79}$$

This is illustrated in Fig. 2, which shows the population of the ground state of the unperturbed hydrogen atom when the atom is exposed to a $\sin^2$-shaped laser pulse of a duration corresponding to five optical cycles, a maximum electric field strength of 10 a.u. (corresponding to a peak intensity of 3.5×10^{18} W/cm^2), and a central frequency ω of 2.0 a.u. (corresponding to a photon energy of about 54 eV). The population is seen to coincide with the result of a corresponding Hermitian calculation. The latter is performed by a split operator scheme on a spherical grid [41,67]. It has also been checked that the methods of Secs. III A–III C all give the same result. Since the amplitudes of the pseudocon-

tinuum states in the expansion in Eq. (38) vanish exponentially after the interaction, it is also seen that the sum of the absolute square of all the amplitudes, $\Sigma_n |d_n^\theta(t)|^2$ in the limit in Eq. (41), converges towards the survival probability of the system. Interestingly, during the interaction this sum, indicated by the dash-dotted curve in the figure, is not a strictly decreasing function of time; in several intervals it increases. These fluctuations are consequences of the fact that the formalism is not Hermitian when only propagation of the "right" state Ψ^θ is considered. The anti-Hermitian part of the representation of the Hamiltonian is the reason why the sum $\Sigma_n |d_n^\theta(t)|^2$, which in general does not represent any physical quantity, is not conserved in time. The anti-Hermitian contribution from the matrix representation of the unperturbed Hamiltonian, $\mathbb{H}_{mn}^\theta - (\mathbb{H}_{nm}^\theta)^* = 2i\delta_{mn} \text{Im}(E_n^\theta)$, will always lead to a decrease in the magnitude of the amplitudes corresponding to pseudocontinuum states since it is never positive $[\text{Im}(E_n^\theta) \leqslant 0]$. The anti-Hermitian contribution from the interaction alternates in sign, however, causing $\Sigma_n |d_n^\theta(t)|$ to increase at certain times. Another manifestation of this phenomenon is the fact that the eigenenergies of the full, time-dependent Hamiltonian, Eq. (57), have, depending on the phase of the field, positive imaginary parts in certain time intervals. In order to avoid this increase in the magnitude of the rotated wave function, He *et al.* [45], who used exterior complex scaling as a way of imposing an absorbing boundary, removed the complex scaling of the interaction term altogether. For stronger fields, the sum $\Sigma_n |d_n^\theta(t)|^2$ may in fact even exceed unity. This clearly demonstrates that it may *not* be interpreted as any probability. Analogously, the integral $\int |\Psi^\theta(\mathbf{r})|^2 dV$ does not have any meaningful physical interpretation either. This disagrees with the statements made in connection with Eq. (15) of Ref. [47]; the equation may hold in the specific case of a single populated bound state, but it is formally incorrect for the general case.

For weaker fields the fluctuations in the above-mentioned sum are absent or at least very small. Since we know that the sum eventually is to converge towards the survival probability of the system, physical information may in this case be extracted from the coefficients d_n^θ also during the interaction with the laser pulse. It has been demonstrated that for atoms exposed to dc fields, the ionization rate may be found directly from the imaginary part of the ground state energy of the full Hamiltonian [27]. Figure 3 demonstrates how ionization rates may be found also for atoms exposed to ac fields through the sum $\Sigma_n |d_n^\theta(t)|^2$. Here a hydrogen atom is exposed to an oscillating electric field with a constant amplitude of 0.1 a.u. (corresponding to a peak intensity of 3.5×10^{14} W/cm^2) between a two-cycle ramp on/off. The frequency ω is 0.7 a.u. (corresponding to the photon energy $\hbar\omega \approx 19$ eV). The sum $\Sigma_n |d_n^\theta|^2$ is shown for three different choices of θ on a semilogarithmic scale along with the probability of being in a bound state (in the velocity gauge). It is clearly seen that after a certain time the three curves are parallel on such a plot and that they all eventually coincide with the final survival probability. Thus we may use this time-dependent sum to assign an ionization rate to the process. This rate may also be extracted from the imaginary part of the quasienergy, ϵ_0^θ, associated with the field-dressed ground state of the Floquet Hamiltonian, cf. Eq. (62), of an
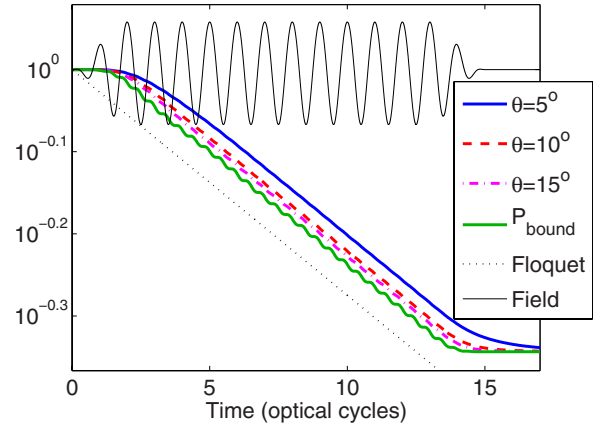

FIG. 3. (Color online) The sum $\Sigma_n |d_n^\theta(t)|^2$, see the caption of Fig. 2, during interaction between a hydrogen atom initially in the ground state and an electric field oscillating with a constant amplitude (indicated by the black curve). The field is "ramped on/off" over a period of two optical cycles. This sum is shown for three choices of θ, namely, from the top, 5° (full blue curve), 10° (dashed red curve), and 15° (dash-dotted magenta curve). The oscillating curve below these three is the population of all bound states in the velocity gauge (full green curve). Finally, the survival probability of the "ground state" of the Floquet Hamiltonian for monochromatic laser light (dotted curve) is also shown. These curves are shown on a semilogarithmic scale in order to demonstrate that they are all parallel, i.e., they all correspond to the same ionization rate. The field has a peak intensity of 3.5×10^{14} W/cm^2, a frequency of 0.7 a.u. (corresponding to the photon energy $\hbar\omega \approx 19$ eV), and a duration corresponding to 15 optical cycles.

atom exposed to a monochromatic field [30]. The corresponding time evolution of the population of this state, $\exp[2 \, \text{Im}(\epsilon_0^\theta)t/\hbar] = \exp(-\Gamma t/\hbar)$, is included in Fig. 3 as a dotted line. As is seen from the figure, the two procedures yield the same ionization rate. In this particular case it is $\Gamma/\hbar = 7.0 \times 10^{-3}$ a.u. $= 2.9 \times 10^{14}$ s^{-1}.

One advantage of complex scaling, compared to the ordinary Hermitian formalism, is that the coupling between bound states and the continuum is adequately described with surprisingly few pseudocontinuum states. In Fig. 4, where again the population of the atomic ground state of hydrogen is considered, this advantage is easily seen. As the number of unrotated pseudocontinuum states increases, the population converges towards that computed using complex rotation—even when the number of unrotated basis states exceeds the number of rotated ones by far. It should further be emphasized that the number of rotated states used in this calculation is not the lowest number possible for convergent results. Longer pulses, corresponding to narrower energy distributions, require a denser set of unrotated pseudocontinuum states. For the cases of complex rotation, on the other hand, each pseudocontinuum state is, as we will discuss in the following section, associated with a broader energy width which makes accurate predictions possible with relatively few states even for pulses with narrow frequency distributions.
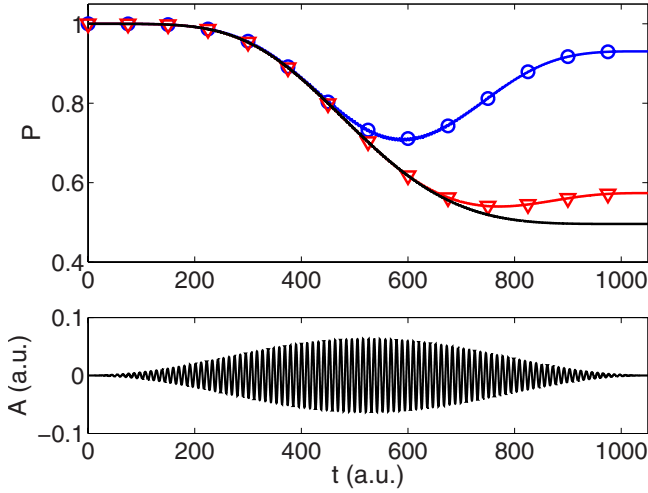
FIG. 4. (Color online) *Upper panel*: The population of the atomic ground state of a hydrogen atom is computed with and without complex scaling. In the latter case the calculation was performed using 50 (blue line with circles) and 100 (red line with triangles) atomic states for each angular symmetry. For $\theta = 20°$ (black line) the corresponding number of states is 30. As seen, the significantly lower number of rotated states gives an accurate population during the entire pulse. The better description is explained by an energy width associated with each rotated pseudocontinuum state. *Lower panel*: The vector potential, corresponding to a peak intensity of 5.0×10^{13} W/cm^2 and carrier frequency of $\omega = 0.6$ a.u.

V. TRANSFORMATION TO THE TRUE CONTINUUM

The fact that convergence of the "right" rotated wave function, with respect to the number of pseudocontinuum states, is achieved faster for higher values of θ may be understood from the relation between rotated pseudocontinuum states and rotated true continuum states. When the energy spectrum of the continuum is discretized through a "box potential," one may somewhat simplified think of each pseudocontinuum state as effectively representing an interval, with a certain width, of the true energies. When complex scaling is imposed, the width of this interval is increased, and as the scaling angle θ increases, so does the energy interval represented by each rotated pseudocontinuum state. This phenomenon is illustrated in Fig. 5, which shows the projections of a particular box normalized complex rotated eigenstate onto rotated continuum functions for the hydrogen atom. The latter behave asymptotically as outgoing plane waves. More specifically the figure shows

$$F_{n,\ell,m}^{\theta}(k) \equiv \int_0^R [\Phi_{n,\ell,m}^{-\theta}(\mathbf{r})]^* \psi_{k,\ell,m}^{\text{out}}(\mathbf{r}e^{i\theta})e^{3i\theta}dV. \quad (80)$$

The left function, $[\Phi_{n,\ell,m}^{-\theta}(\mathbf{r})]^*$, coincides with $\Phi_{n,\ell,m}^{\theta}$ since all complexity arises from the complex scaling in this case. The rotated outgoing wave is defined by

$$\psi_{k,\ell,m}^{\text{out}}(\mathbf{r}e^{i\theta}) = \frac{1}{\sqrt{2}}[g_{l,k}(re^{i\theta}) + if_{l,k}(re^{i\theta})]Y_{\ell m}(\Omega), \quad (81)$$

where $f_{\ell,k}$ and $g_{\ell,k}$ are the regular and irregular Coulomb wave functions, respectively. This representation is chosen
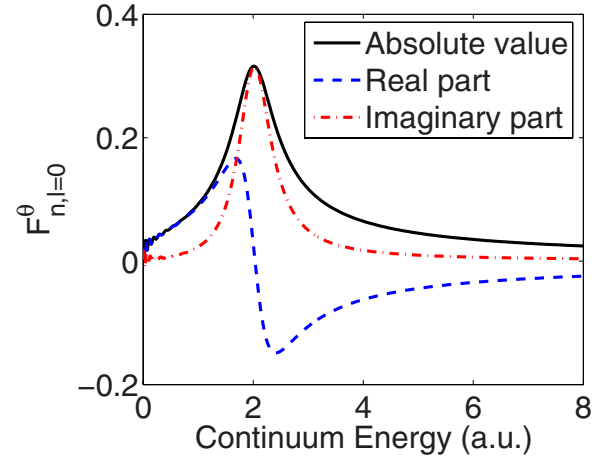

FIG. 5. (Color online) The figure shows the projection of a box normalized pseudocontinuum state onto rotated analytical continuum states with outgoing, plane wave asymptotic behavior, i.e., $F_{n,\ell,m}^{\theta}$ in Eq. (80). The x axis shows the energy of the analytical continuum states. The half width of the distribution increases with increasing θ. More specifically, the width of $|F_{n,\ell,m}^{\theta}|^2$ coincides quite well with twice the absolute value of the imaginary part of the energy of the box normalized pseudocontinuum state, Im(E_n). This particular case corresponds to the $\ell = 0$ channel with the scaling angle $\theta = 5°$ and a box state with Re(E_n) = 2.0 a.u.

because of its behavior for large r; it falls off exponentially, whereas any other linear combination of the two Coulomb functions would grow exponentially. A program for calculating these functions numerically for complex arguments is provided in Ref. [68]. The eigenenergy corresponding to the box normalized state in Fig. 5 is complex, whereas the eigenenergies of the $\psi_{k,\ell,m}^{\text{out}}$ states are real. For the illustration in Fig. 5 a "box energy" E_n^{θ} with a real part of 2.0 a.u is chosen, the angular quantum number ℓ is zero and the scaling angle θ is 5°. The figure clearly shows a broad distribution in the projection $F_{n,\ell=0}^{\theta}$ centered around the real part of E_n^{θ}. The width of the distribution is dictated by the scaling angle θ.

If we, in the $\ell = 0$ channel, neglect the Coulomb potential, both the outgoing wave and the pseudocontinuum states have very simple analytical forms; the reduced wave functions are $r \exp(i\theta)\psi_{k,\ell=0}^{\text{out}} = \sqrt{2/\pi}\exp[ikr\exp(i\theta)]$ and $r \exp(i\theta)\Phi_{n,\ell,m}^{\theta}(\mathbf{r}) = \sqrt{2/R}\sin(k_n r)$ with $k_n = n\pi/R$. The latter wave function is thus unaffected by the complex scaling, although the energy E_n^{θ} is, as in the Coulomb case, complex: $E_n^{\theta} = (\hbar k_n)^2 \exp(-2i\theta)/2m$, cf., the relation in Eq. (20). In this context, the projections $F_{n,\ell}^{\theta}$ may be found analytically:

$$|F_{n,\ell=0}^{\theta}|^2 = \frac{2\hbar^2}{\pi m R} \frac{|E_n^{\theta}|}{|E_n^{\theta}|^2 + \varepsilon_k^2 - 2|E_n^{\theta}|\varepsilon_k \cos(2\theta)} \quad (82)$$

with $\varepsilon_k \equiv (\hbar k)^2/2m$. Although the neglect of the Coulomb potential is a rather crude approximation, the simple function of Eq. (82) exhibits most of the relevant features of the one which includes the Coulomb potential. For fixed "box energy" E_n^{θ}, the function has its maximum value for

$$\varepsilon_k = |E_n^\theta|\cos(2\theta) = \text{Re}(E_n^\theta), \qquad (83)$$

and the half width is

$$\frac{\Delta\varepsilon_k}{2} = |E_n^\theta|\sin(2\theta) = \text{Im}(E_n^\theta). \qquad (84)$$

Numerical inspection shows that the identification of the maximum of $|F_{n,\ell}^\theta|^2$ with the real part of E_n^θ, as well as that of the half width of $|F_{n,\ell}^\theta|^2$ with the imaginary part of E_n^θ, remain very reasonable estimates also when the Coulomb potential is included.

A. Obtaining the true wave function through back rotation

As we have seen, the wave function may be well-represented with rather few basis states in a complex rotated context. This raises the question of whether information contained in the wave function is lost when complex scaling is imposed—at least from a numerical point of view. Analytically, all information about the system should, in principle, be obtainable from $\Psi(\mathbf{r}e^{i\theta})$ simply by a variable transformation back to the unrotated coordinate, i.e., $\mathbf{r}\exp(-i\theta)$ is used instead of $\mathbf{r}$ in the complex rotated wave function, as suggested in Ref. [46]. It is not obvious, however, to what extent this is feasible in practice. To illustrate how it can be done, we use as an example the same simple case as above, namely an isotropic wave subject to no interaction. If we start out with a wave packet with the initial momentum distribution $\varphi(k)$, its evolution is given by

$$\Psi(r,t) = \int_0^\infty \varphi(k)\exp\left(-i\frac{\hbar k^2}{2m}t\right)\sqrt{\frac{2}{\pi}}\frac{\sin(kr)}{r}dk\,Y_{0,0}. \qquad (85)$$

With no boundary condition imposed, the corresponding complex rotated wave function, $\Psi^\theta(r,t)$, is obtained by the usual substitution. Note that in this representation, our basis functions, $\sqrt{2/\pi}\sin[kr\exp(i\theta)]/r\exp(i\theta)$, grow exponentially with r. However, a propagating wave packet may still be well-represented by these functions. The box representation of this rotated wave function is found as

$$\Psi_{\text{box}}^\theta(r,t) = \sum_n c_n^\theta \exp\left(-i\frac{\hbar k_n^2 e^{-2i\theta}}{2m}t\right)$$
$$\times \sqrt{\frac{2e^{-i\theta}}{R}}\frac{\sin(k_n r)}{re^{i\theta}}Y_{0,0}, \quad k_n = \frac{n\pi}{R}, \quad (86)$$

where the coefficients c_n^θ are obtained from Ψ^θ by $c_n^\theta = \int_0^\infty \varphi(k)\int_0^R \sqrt{2/R}\sin(k_n r)\sqrt{2/\pi}\sin(kre^{i\theta})\exp(3i\theta/2)drdk$. The integral over r is easily done analytically. Now, if Eq. (86) is a good representation of the rotated wave function, the unrotated wave function should be reobtainable from Ψ_{box}^θ by back substitution:
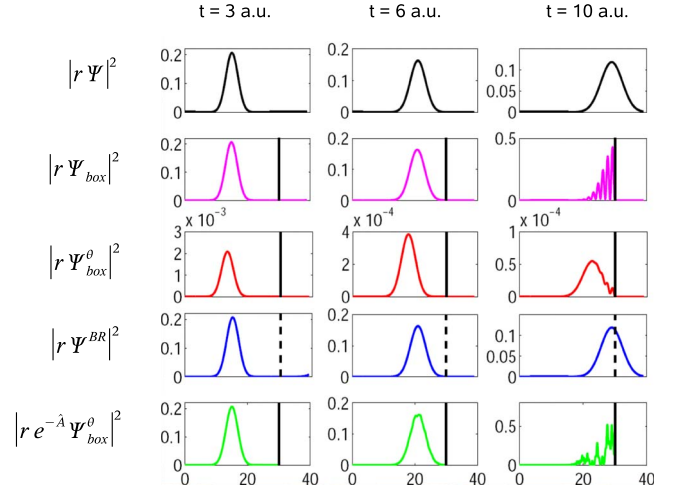

FIG. 6. (Color online) The propagation of an isotropic outgoing spherical wave subject to no potential in five different representations. From top to bottom: The true wave function $|r\Psi|^2$, Eq. (85), an unrotated box representation of the wave $|r\Psi_{\text{box}}|^2$, the corresponding representation of the complex rotated wave $|r\Psi_{\text{box}}^\theta|^2$ in the box, Eq. (86), the "back-rotated" wave function $|r\Psi^{\text{BR}}|^2$ obtained via a variable substitution, Eq. (87), and finally, the back-rotated wave function obtained by applying the rotation operator, Eq. (89). The scaling angle θ is here 5°. The wave functions are shown at three instances, namely $t=3$ a.u. (left), $t=6$ a.u. (middle), and $t=10$ a.u. (right). The vertical bars in the four lowest panels indicate the box size, which is $R=30$ a.u.

$$\Psi^{\text{BR}}(r,t) = \sum_n c_n^\theta \exp\left(-i\frac{\hbar k_n^2 e^{-2i\theta}}{2m}t\right)\sqrt{\frac{2e^{-i\theta}}{R}}\frac{\sin(k_n re^{-i\theta})}{r}Y_{0,0}. \qquad (87)$$

Although complex scaling is not simply a variable substitution when a confining potential is imposed, this "back substitution" should still give us the true wave function back as long as it has not reached the boundary. The fourth panel in Fig. 6 demonstrates that the unrotated wave function may indeed be obtained from the rotated one in this way. It also demonstrates, in agreement with Ref. [42], that complex rotation may provide a description superior to the unrotated one. Figure 6 will be discussed in detail shortly.

The downside of this "back substitution" method is its lack of numerical stability. It is evident that since the basis functions at hand diverge as r becomes large, the upper limit of the integration cannot be too large when projections and expectation values are calculated in practice with these basis functions. However, it must be chosen large enough to actually include the wave packet.

B. Restoring the wave function using the rotation operator

The rotation operator formalism, Eqs. (3)–(11), represents an alternative way to perform the back rotation. By diagonalizing the operator $\hat{A} = -\theta(\mathbf{r}\cdot\mathbf{p} + \mathbf{p}\cdot\mathbf{r})/2\hbar$, the exponent of the rotation operator, in a basis set consisting of, e.g., B splines, we obtain a discrete set of eigenvalues, a_k, and eigenfunctions, $\alpha_k(r)$, i.e., a spectral representation of the

rotation operator. Since $\hat{A}$ is Hermitian, the eigenfunctions are orthogonal according to the ordinary Hermitian inner product. Formally, with normalized eigenfunctions, the rotation operator may now be written as

$$e^{\pm\hat{A}} = \sum_k e^{\pm a_k}|\alpha_k\rangle\langle\alpha_k|, \tag{88}$$

which leads to the following expression for the back-rotated wave function:

$$e^{-\hat{A}}\Psi^\theta = \sum_{k=k_{\min}}^{k_{\max}} e^{-a_k}\left[\int [\alpha_k(r)]^*\Psi^\theta(\mathbf{r})r^2dr\right]\alpha_k(r). \tag{89}$$

Analogous to adjusting the upper integration limit in the previous example, the sum in Eq. (89) may have to be truncated such that $-a_k$ does not become too large. This is due to the fact that the eigenvalue appears in the exponent, which causes the sum to be very sensitive to numerical uncertainties in the higher values of $-a_k$. To determine this upper limit, inspection of whether the norm of the resulting wave function is unity may serve as a check of accuracy and completeness.

In Fig. 6 the propagation of a spherical, outgoing wave packet which is not subject to any potential is shown in five different representations. The first row corresponds to the actual, unrotated wave function, Eq. (85), at three different times. The second row is a box representation of the unrotated wave function, whereas the third row shows the corresponding complex rotated wave function in the same box, Eq. (86). The back-rotated wave function obtained from a direct variable substitution, Eq. (87), is shown in the fourth row, and the final row shows the back-rotated wave function calculated using the rotation operator, Eq. (89). In Fig. 6, the rotation of the Jacobian (r^2) is not included in the notation since it only constitutes a phase factor which does not affect the absolute value. We see that $|r\Psi_{\text{box}}|^2$, second row, is strongly affected by unphysical reflections when the wave packet reaches the box boundary. Referring to the wave packet on the third row, $|r\Psi_{\text{box}}^\theta|^2$, which does not represent any physics, we see that it is strongly distorted compared to the other representations. This is due to the suppression of high momentum components; the absolute values of the time-dependent factors in the expansion in Eq. (86), $|\exp(-i\hbar k_n^2 e^{-2i\theta}t/2m)| = \exp[-\hbar k_n^2 \sin(2\theta)t/2m]$, are seen to vanish more rapidly for higher values of k_n. This distortion delays the wave packet's arrival to the boundary and therefore postpones the appearance of reflection effects. Interestingly, since the "backwards rotated" basis functions, proportional to $\sin[k_n r \exp(-i\theta)]/r$, are nonzero at the boundary, Ψ^{BR} on the fourth row may reproduce the true wave function from Ψ_{box}^θ even at the boundary and beyond. Hence as is clearly seen by comparing the second and fourth row of the figure, a rotated wave function in a box may be able to represent the true wave function far better than an unrotated wave function in the same box, cf. Ref. [42]. Since the rotation operator representation is only well-defined in the space spanned by the B splines, this behavior is not reproduced by this method. As we see in row five, the wave function becomes unphysical as the true wave function reaches the
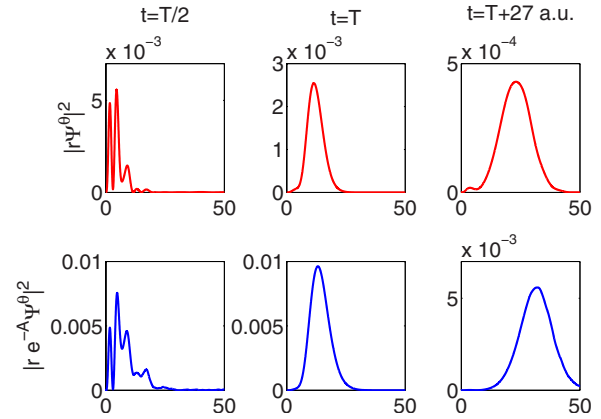

FIG. 7. (Color online) The radial part of the wave function for the $\ell=1$ channel of the wave function corresponding to a hydrogen atom exposed to a $\sin^2$-shaped laser pulse of a duration T corresponding to four optical cycles. The central frequency is $\omega = 0.7$ a.u., and the peak intensity of the field is 3.5×10^{14} W/cm^2. The upper panels correspond to the wave function rotated by 5°, and the lower ones correspond to the back-rotated, physical wave function. The times correspond to, from left to right, when the field intensity is at its maximum, immediately after the interaction and about 27 atomic time units after the interaction is over. Note that the scales of the y axes differ between the upper and lower panels.

boundary, but up to this point the method works well.

Returning to the less trivial case in which the Coulomb potential is included, it should be possible also here to obtain the true continuum wave function from the rotated one. As an example, a hydrogen atom exposed to a 4-cycle laser pulse of central frequency $\omega=0.7$ a.u. (corresponding to a photon energy of ~19 eV) and maximum electric field strength $E_0=0.1$ a.u. (corresponding to a peak intensity of $I = 3.5\times10^{14}$ W/cm^2) has been studied. Figure 7 shows the time evolution of the $\ell=1$ component of the wave function. Both the rotated and back-rotated wave functions are shown during, immediately after, and at a time of about 27 atomic time units, 0.65 fs, after the interaction is over. The scaling angle θ is here 5°. The back-rotated wave function is obtained through Eq. (89).

As mentioned, the ability to reconstruct the true wave function enables us to obtain information about the photoelectron spectrum. For instance, the energy distribution of the ionized electron, $dP_{\text{ion}}/d\varepsilon$, may be found. This is shown for the above case in Fig. 8 along with the corresponding prediction from Eq. (43), where the $[d_n^{-\theta}(t)]^*d_n^\theta(t)$'s are obtained through Floquet theory, Eqs. (71) and (72). The results of the two methods are clearly seen to coincide. For this specific case a clear peak corresponding to the absorption of one photon may be observed. A smaller peak indicative of two photon ionization may also be seen on a semilogarithmic plot.

VI. CONCLUSION

The formalism of inner products in the context of uniform complex scaling was reviewed in detail. We showed that it may be formulated such that all physical quantities coincide
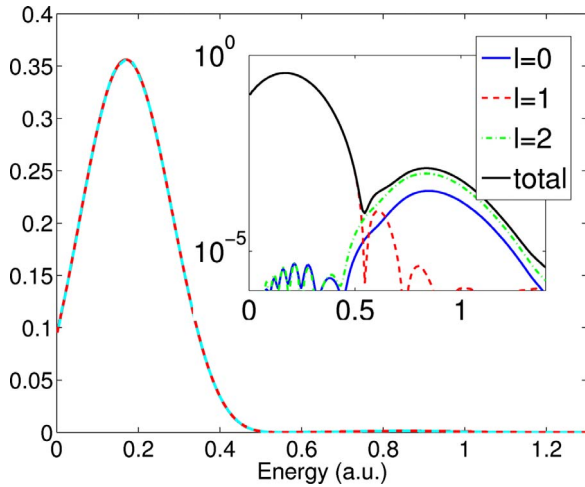
FIG. 8. (Color online) The photoelectron spectrum for the same system as in Fig. 7. The full (red) curve is obtained by using Eq. (43) where the coefficients are calculated using Floquet theory, and the dashed (magenta) curve is obtained by rotating back the rotated wave function and projecting it onto continuum states, $dP_{\text{ion}}/d\varepsilon = \Sigma_\ell |\langle \psi_{l,E}| \exp(-\hat{A})|\Psi^\theta(T)\rangle|^2$. The inset shows the latter on a semilogarithmic scale so that a peak corresponding to absorption of two photons may be seen clearly. The colored curves in the inset are the contributions from the different channels; the blue, full curve corresponds to the $\ell=0$ channel, the red, dashed curve to $\ell=1$, and the green, dash-dotted curve corresponds to $\ell=2$.

with the results of a corresponding Hermitian calculation. Specifically, left and right wave functions are expanded in left or right eigenfunctions, respectively, to some complex scaled operator. The left eigenfunctions are obtained in the

same manner as the right ones, but with opposite sign of the scaling angle. In the case of dynamical systems, the right wave function is found by propagation with the rotated Hamiltonian, $H^\theta(t)$, whereas the left wave function is obtained from the Hamiltonian with the opposite rotation, $H^{-\theta}(t)$.

Furthermore, we demonstrated that uniform complex scaling has considerable advantages when calculating ionization probabilities. Numerical convergence is obtained faster when we propagate with the rotated Hamiltonian H^θ for the right rotated wave function than for the unrotated one for two reasons. First, the whole spectrum of continuum energies is covered by fewer pseudocontinuum states. Second, unphysical reflection effects at the boundary of the confining potential are, to a large extent, avoided. An important point here is that the probability of finding the system in any bound state can be obtained from the right rotated wave function alone.

Finally, physical information about the continuum state was shown to be obtainable from the complex rotated wave function by imposing the opposite variable substitution, as well as by back-rotation with a spectral representation of the complex rotation operator. It was further found that the Floquet formalism offers a possibility to directly form the inner product of the left and right wave function at any time from the eigenstates to the *time-independent* Floquet matrix, thereby a numerically much more robust path to the same information is obtained.

[1] W. Reinhardt, Annu. Rev. Phys. Chem. **33**, 223 (1982).
[2] B. Junker, Adv. At. Mol. Phys. **18**, 208 (1982).
[3] Y. K. Ho, J. Phys. B **10**, L373 (1977).
[4] Y. K. Ho, J. Phys. B **12**, 387 (1979).
[5] Y. K. Ho, Phys. Rev. A **48**, 3598 (1993).
[6] K. T. Chung and B. F. Davis, Phys. Rev. A **26**, 3278 (1982).
[7] E. Lindroth, Phys. Rev. A **49**, 4473 (1994).
[8] D. R. DeWitt, E. Lindroth, R. Schuch, H. Gao, T. Quinteros, and W. Zong, J. Phys. B **28**, L147 (1995).
[9] D. Nikolic and E. Lindroth, J. Phys. B **37**, L285 (2004).
[10] D. Wintgen and D. Delande, J. Phys. B **26**, L399 (1993).
[11] A. Bürgers, D. Wintgen, and J.-M. Rost, J. Phys. B **28**, 3163 (1995).
[12] S. Berkovic, R. Krivec, V. Mandelzweig, and L. Stotland, Phys. Rev. A **55**, 988 (1997).
[13] T. N. Rescigno and V. McKoy, Phys. Rev. A **12**, 522 (1975).
[14] E. Lindroth, Phys. Rev. A **52**, 2737 (1995).
[15] J. L. Sanz-Vicario, E. Lindroth, and N. Brandefelt, Phys. Rev. A **66**, 052713 (2002).
[16] W. Zong, R. Schuch, E. Lindroth, H. Gao, D. R. DeWitt, S. Asp, and H. Danared, Phys. Rev. A **56**, 386 (1997).
[17] S. Mannervik, D. DeWitt, L. Engström, J. Lidberg, E. Lindroth, R. Schuch, and W. Zong, Phys. Rev. Lett. **81**, 313

(1998).
[18] P. Glans, E. Lindroth, N. R. Badnell, N. Eklöw, W. Zong, E. Justiniano, and R. Schuch, Phys. Rev. A **64**, 043609 (2001).
[19] E. Lindroth, H. Danared, P. Glans, Z. Pešić, M. Tokman, G. Vikor, and R. Schuch, Phys. Rev. Lett. **86**, 5027 (2001).
[20] M. Tokman, N. Eklöw, P. Glans, E. Lindroth, R. Schuch, G. Gwinner, D. Schwalm, A. Wolf, A. Hoffknecht, A. Müller, and S. Schippers, Phys. Rev. A **66**, 012703 (2002).
[21] S. Madzunkov, E. Lindroth, N. Eklöw, M. Tokman, A. Paál, and R. Schuch, Phys. Rev. A **65**, 032505 (2002).
[22] T. Mohamed, D. Nikolic, E. Lindroth, S. Madzunkov, M. Fogle, M. Tokman, and R. Schuch, Phys. Rev. A **66**, 022719 (2002).
[23] M. Fogle, N. Eklöw, E. Lindroth, T. Mohamed, R. Schuch, and M. Tokman, J. Phys. B **36**, 2563 (2003).
[24] D. Nikolic, E. Lindroth, S. Kieslich, C. Brandau, S. Schippers, W. Shi, A. Müller, G. Gwinner, M. Schnell, and A. Wolf, Phys. Rev. A **70**, 062723 (2004).
[25] S. Kieslich, S. Schippers, W. Shi, A. Müller, G. Gwinner, M. Schnell, A. Wolf, E. Lindroth, and M. Tokman, Phys. Rev. A **70**, 042714 (2004).
[26] A. Maquet, Shih-I Chu, and W. P. Reinhardt, Phys. Rev. A **27**, 2946 (1983).

[27] A. Scrinzi, Phys. Rev. A **61**, 041402(R) (2000).

[28] I. A. Ivanov and Y. K. Ho, Phys. Rev. A **69**, 023407 (2004).

[29] J. H. Shirley, Phys. Rev. **138**, B979 (1965).

[30] S. I. Chu and W. P. Reinhardt, Phys. Rev. Lett. **39**, 1195 (1977).

[31] C. R. Holt, M. G. Raymer, and W. P. Reinhardt, Phys. Rev. A **27**, 2971 (1983).

[32] S. I. Chu and D. A. Telnov, Phys. Rep. **390**, 1 (2004).

[33] N. Elander and E. Yarevsky, Phys. Rev. A **57**, 3119 (1998).

[34] F. Morales, C. W. McCurdy, and F. Martin, Phys. Rev. A **73**, 014702 (2006).

[35] C. W. McCurdy, T. N. Rescigno, and D. Byrum, Phys. Rev. A **56**, 1958 (1997).

[36] T. N. Rescigno, M. Baertschy, D. Byrum, and C. W. McCurdy, Phys. Rev. A **55**, 4253 (1997).

[37] D. A. Horner, F. Morales, T. N. Rescigno, F. Martín, and C. W. McCurdy, Phys. Rev. A **76**, 030701(R) (2007).

[38] T. N. Rescigno, W. Vanrose, D. A. Horner, F. Martín, and C. W. McCurdy, J. Electron Spectrosc. Relat. Phenom. **161**, 85 (2007).

[39] E. S. Smyth, J. S. Parker, and K. T. Taylor, Comput. Phys. Commun. **114**, 1 (1998).

[40] M. D. Feit, J. A. Fleck, and A. Steiger, J. Comput. Phys. **47**, 412 (1982).

[41] J. P. Hansen, T. Sørevik, and L. B. Madsen, Phys. Rev. A **68**, 031401(R) (2003).

[42] S. D. Parker and C. W. McCurdy, Chem. Phys. Lett. **156**, 483 (1989).

[43] C. W. McCurdy, C. K. Stroud, and M. K. Wisinski, Phys. Rev. A **43**, 5980 (1991).

[44] C. W. McCurdy, D. A. Horner, and T. N. Rescigno, Phys. Rev. A **65**, 042714 (2002).

[45] F. He, C. Ruiz, and A. Becker, Phys. Rev. A **75**, 053407 (2007).

[46] A. Scrinzi and B. Piraux, Phys. Rev. A **58**, 1310 (1998).

[47] T. Grosges, B. Piraux, and H. Bachau, Phys. Rev. A **60**, 1371 (1999).

[48] G. Lagmago Kamta, T. Grosges, B. Piraux, R. Hasbani, E. Cormier, and H. Bachau, J. Phys. B **34**, 857 (2001).

[49] A. Buchleitner, D. Deland, and J.-C. Gay, J. Opt. Soc. Am. B **12**, 505 (1995).

[50] N. Moiseyev, P. R. Certain, and F. Weinhold, Mol. Phys. **36**, 1613 (1978).

[51] I. Gilary, A. Fleischer, and N. Moiseyev, Phys. Rev. A **72**, 012117 (2005).

[52] E. Merzbacher, *Quantum Mechancis*, 3rd ed. (Wiley, New York, 1998), p. 39.

[53] N. Moiseyev, Phys. Rep. **302**, 212 (1998).

[54] A. Fleischer and N. Moiseyev, Phys. Rev. A **72**, 032103 (2005).

[55] I. Gilary, P. R. Kaprálová-Žd'ánská, and N. Moiseyev, Phys. Rev. A **74**, 052505 (2006).

[56] Y. Ho, Phys. Rep. **99**, 1 (1983).

[57] C. deBoor, *A Practical Guide to Splines* (Springer-Verlag, New York, 1978).

[58] W. R. Johnson and J. Sapirstein, Phys. Rev. Lett. **57**, 1126 (1986).

[59] H. Bachau, E. Cormier, P. Decleva, J. E. Hansen, and F. Martin, Rep. Prog. Phys. **64**, 1815 (2001).

[60] W. H. Press, B. P. Flannery, S. A. Teukolsky, and W. T. Vetterling, *Numerical Recipes: The Art of Scientific Computing (FORTRAN Version)* (Camebridge University Press, Camebridge, England, 1989).

[61] G. Floquet, Ann. Scuola Norm. Sup. Pisa, Cl. Sci. **12**, 47 (1883).

[62] T. S. Ho and S. I. Chu, Chem. Phys. Lett. **141**, 315 (1987).

[63] T. S. Ho, S. I. Chu, and J. V. Tietz, Chem. Phys. Lett. **96**, 464 (1983).

[64] Y. Huang and S. I. Chu, Chem. Phys. Lett. **225**, 46 (1994).

[65] P. G. Burke, P. Francken, and C. J. Joachain, J. Phys. B **24**, 761 (1991).

[66] J. Rao, B. Li, and K. T. Taylor, J. Phys. B **32**, L145 (1999).

[67] T. K. Kjeldsen, L. A. A. Nikolopoulos, and L. B. Madsen, Phys. Rev. A **75**, 063427 (2007).

[68] J. Thompson and A. Barnett, Comput. Phys. Commun. **36**, 363 (1985).